8-2015

Mechanics of electrode materials in lithium battery applications.

Jubin Chen
University of Louisville

MECHANICS OF ELECTRODE MATERIALS IN LITHIUM BATTERY APPLICATIONS

By

Jubin Chen

A Dissertation
Submitted to the Faculty of the
J. B. Speed School of Engineering of the University of Louisville
in Partial Fulfillment of the Requirements
for the Degree of

Doctor of Philosophy

in Mechanical Engineering

Department of Mechanical Engineering
University of Louisville
Louisville, Kentucky

August 2015

MECHANICS OF ELECTRODE MATERIALS IN LITHIUM BATTERY APPLICATIONS

By

Jubin Chen

A Dissertation Approved on

August 7, 2015

by the following Dissertation Committee:

_____

Dissertation Director

Dr. Thomas A. Berfield

_____

Dr. Sam Park

_____

Dr. Zhihui Sun

_____

Dr. Stuart J. Williams

DEDICATION

This thesis is dedicated to my parents

Yongfu Chen and Xiulan Wei

My wonderful wife and sons

Aiqin Fang

Chris Chen and Charles Chen

ACKNOWLEDGEMENTS

First of all, I would like to acknowledge my advisor Dr. Thomas A. Berfield without whom none of this would have been possible. I appreciate him for taking me into his group, teaching me to think independently, to do research, and to have a vision for the future. He is always there for scientific discussions and research difficulties. His insight, support, and encouragement during these years have been invaluable.

Second, I would like to thank my committee members Dr. Zhihui Sun, Dr. Sam Park, and Dr. Stuart J. Williams for their valuable advice and suggestions on my research. I also would like to thank all current and former group members. Dr. Daniel A. Porter and Trung Hoang whom discuss with me and give me valuable suggestions.

Third, I would like to acknowledge our collaborators Dr. Arjun K. Thapa from Conn Center of University of Louisville. Without their expertise in battery assembly and test, it would be very hard for me to get some of the experimental results.

Last but not least, I would like to acknowledge my parents for making many sacrifices in supporting me to pursue my studies thousands of miles away from home. I also would like to express my deep love and appreciations to my wife Aiqin Fang for always encouraging and supporting me in the tough times. A special thanks to my sweet sons Chris and Charles for bringing so much joy and happiness to my life.

ABSTRACT

MECHANICS OF ELECTRODE MATERIALS IN LITHIUM

BATTERY APPLICATIONS

August 4, 2015

Jubin Chen

During lithiation and detlithiation, substantial volumetric changes occur within the electrode materials used for rechargeable lithium batteries. The magnitude of these deformations is inherently linked to the electrical capacity of the battery electrical capacity, which tends to degrade with repeated cycling. In this dissertation, the relationship between electrical discharge capacity and mechanical deformation state is examined using *in-situ* imaging of the working electrode surface within a custom CR2032 coin cell lithium battery. Digital image correlation is used to quantify electrode strains throughout the discharge-charge process. The effect of constraint due to substrate stiffness is investigated for two film materials: traditional graphite and a carbon nanotube based composite. Results for all cases show that as discharge capacity decreases with repeated cycling, increasing residual electrode strains are observed. The thin, compliant foil substrates allowed over double the bi-axial strain state to be induced within electrodes, compared to that found for the thick copper disk substrates under the same electrical cycling conditions. While this work shows that substrates play a significant role in strain development, additional tests are done to

investigate the effects of adhesion quality between electrode films and substrates on electrochemical performance of lithium batteries. These effects are probed using a laser spallation technique to quantify the adhesion strength between film and substrate layer. The benefits of surface treatment designed to improve adhesion are also investigated. At last, delamination test of graphite electrode film "sandwiched" by copper substrate are performed. And the results show that surface treatment by mechanical or chemical manner can improve the adhesion dramatically.

TABLE OF CONTENTS

LIST OF TABLES

LIST OF FIGURES

CHAPTER I

INTRODUCTION: BACKGROND LITERATURE AND MOTIVATIONS

1.1 Overview of Dissertation

In this dissertation, the relationship between electrical discharge capacity and mechanical deformation state is examined using *in-situ* imaging of the anode surface within a custom CR2032 coin cell battery. Digital image correlation (DIC) is used to quantify electrode strains throughout the charge-discharge process. The effect of constraint due to substrate stiffness is investigated for two types of materials: traditional graphite and a carbon nanotube based composite. Results for all cases show that as discharge capacity decreases with repeated cycling, increasing residual anode strains are observed. Thin, compliant foil substrates allowed over double the bi-axial strain state to be induced within anodes, compared to that found for the thick copper disk substrates under the same electrical cycling conditions. The magnitude of these deformations is inherently linked to the electrical capacity of the battery electrical capacity, which tends to degrade with repeated cycling.

In addition to the constraint supplied by the substrates playing a significant role in strain development, additional tests are performed to investigate the effects related to electrode-substrate adhesion quality. These effects are probed using a laser spallation technique to quantify the adhesion strength between sputtered film electrodes and the substrate layer,

and via a double cantilever beam delamination test for slurry-formed electrodes. In this work, the benefits of surface treatment processes designed to improve adhesion are assessed and related to coin cell cycling electrochemical performance.

1.2 Lithium Ion Battery Introduction and Working Principle

Currently there is a large demand for high performance lithium ion battery fueled by strong growth in the consumer electronics, power tools, and automotive industries. [1-3] Lithium-ion batteries are highly desirable for these applications due to their outstanding energy-to-weight ratios, their lack of memory effect, and their slower charge loss rate than other battery technologies. Future advances in lithium ion battery performance will likely come from new material developments and optimization of the coupled chemical, electrical, and mechanical interactions that take place within these rechargeable power storage units. [54-56] Selection of the anode material is one of the key considerations affecting lithium ion battery capacity and performance degradation, as these issues are intrinsically related to break-down mechanisms occurring at the material microstructure level. [57-60]

Lithium-ion batteries have several advantages over other battery systems: They are capable of being recharged hundreds of times. They have a higher energy density than most other types of rechargeable batteries which means, that for their size or weight, they can store more energy than other rechargeable batteries. They also operate at higher voltages than other rechargeable batteries, typically higher than 3 volts for lithium-ion vs. 1.2 volts for NiMH or NiCd. Lithium-ion batteries also have a lower self-discharge rate than other types of rechargeable batteries, meaning that once charged they retain their charge for a longer time. In fact, lithium-ion batteries can retain most of their charge even after months of

storage. These attributes make lithium-ion batteries an excellent option for mobile power supply applications.

Lithium-ion batteries also have some issues and challenges. [11,12] First of all, battery capacity will decrease with the number of the cycles and internal resistance tends to increase with the cycle count. Secondly, anode and cathode materials, especially with silicon as anode can generate significant cracking, leading to performance degradation and possible failure of the battery. Thirdly, lithium ion batteries have demonstrated safety issues, including being prone to short-circuiting and heat generation when overcharged which possibly can result in leakage, fire or even explosion. [13]

The three primary components of a lithium ion battery are the anode, the cathode, and the electrolytes. An anode is an electrode through which electric current flows into the device. On the other hand, a cathode is an electrode through which electric current flows out of the device. Electrolytes in lithium ion batteries are usually liquid substances that act as a medium to conduct electricity between the anode and cathode. During discharge, lithium ions carry the current from the negative to positive electrode, while during charging, an external power source applied an over voltage, forcing the current to pass in the reverse direction. Traditionally, graphite has been widely used as the anode for lithium ion batteries due to its ease of processing and low cost. However, graphitic anodes have several drawbacks, such as low specific capacity, that opens up the window for alternative materials.

The cathode is typically made from one of three materials: lithium cobalt oxide, lithium iron phosphate or lithium manganese oxide [14].

Electrolytes play an important role in lithium ion batteries. The electrolyte is typically a mixture of organic carbonates, such as ethylene carbonate or diethyl carbonate, which also contains complexes of lithium ions such as lithium hexafluorophosphate (LiPF6) [15].

A lithium ion battery contains the anode, the cathode and the electrolyte. During the charge and discharge processes in rechargeable batteries, lithium ions are inserted or extracted from interstitial space between atomic layers within the active material of the battery.

During charging, the positive material is oxidized and the negative material is reduced. In this process, lithium ions are de-intercalated from the positive material and intercalated into the negative material. The reverse process is present during a discharge cycle.

Charge/Discharge chemical reactions:

Positive: $LiXX0_2 \leftrightarrow Li_{1-x}XXO_2 + Li^+ + xe^-$

Negative: $C + xLi^+ + xe^- \leftrightarrow Li_xC$

Overall: $LiXX0_2 + C \leftrightarrow Li_xC + Li_{1-x}XXO_2$

XX indicates various combining elements including cobalt, manganese and etc.

The working principle of lithium ion battery is shown in Figure 1.1.

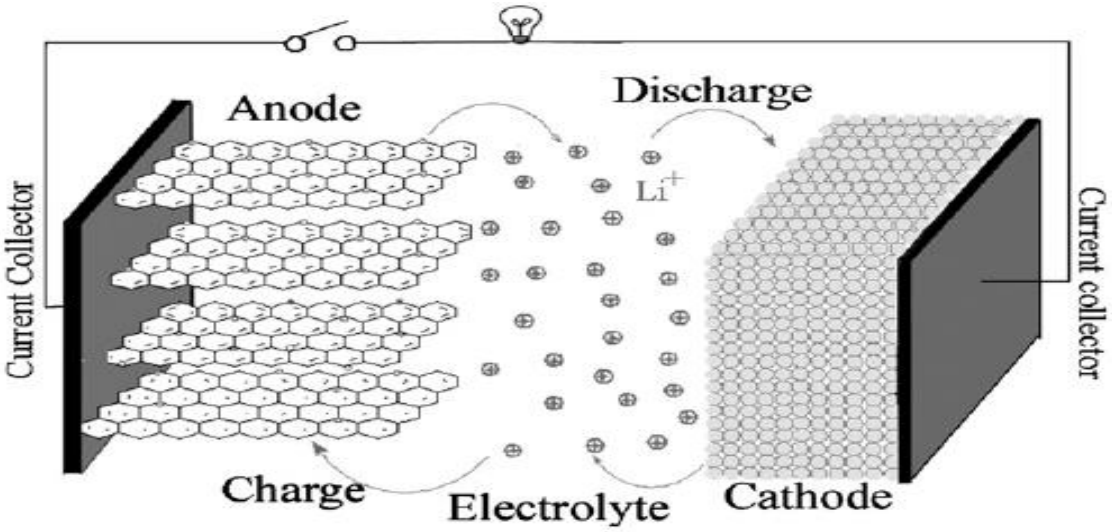

Figure 1.1. Lithium ion battery diagram [16]

1.3 Influence of Electrode Materials on Battery Performance

Graphite has served as the standard anode choice for the first generations of mass produced lithium ion batteries, primarily due to its cost effectiveness [17]. Some of the major limitations of graphite include its relatively low specific capacity (only 372 $mAhg^{-1}$), and substantial irreversible capacity losses during the initial charge-discharge cycles [18-20]. A major source of irreversible capacity loss is the formation of a solid electrolyte interface (SEI) film on the anode surface, the prevalence of which is directly related to the Brunauer-Emmett-Teller (BET) surface area and anode material density [19-24].

Researchers are continuously exploring alternative anode materials of lithium ion batteries include pure elements, alloys, composite materials, metal oxides and so on. [25-27] Promising among these are nanostructured composite material electrodes that have been developed in recent years. Some examples include, Cui, et al. [28], who investigated

carbon-silicon nanowire electrodes which demonstrated high charge capacity (around 2000mAh/g) and good cycling life while also reducing the associated volumetric changes. Higher specific capacity means more electric charge cell can be stored, so the portable devices can be more lightweight and convenient, electrical cars can cover longer road trips with one charge, etc.. Silicon has a theoretical specific capacity that is over 4000mAhg^{-1}, is the highest to date among all the natural materials. Figure 1.2 shows the capacity of several potentially viable elements [29].

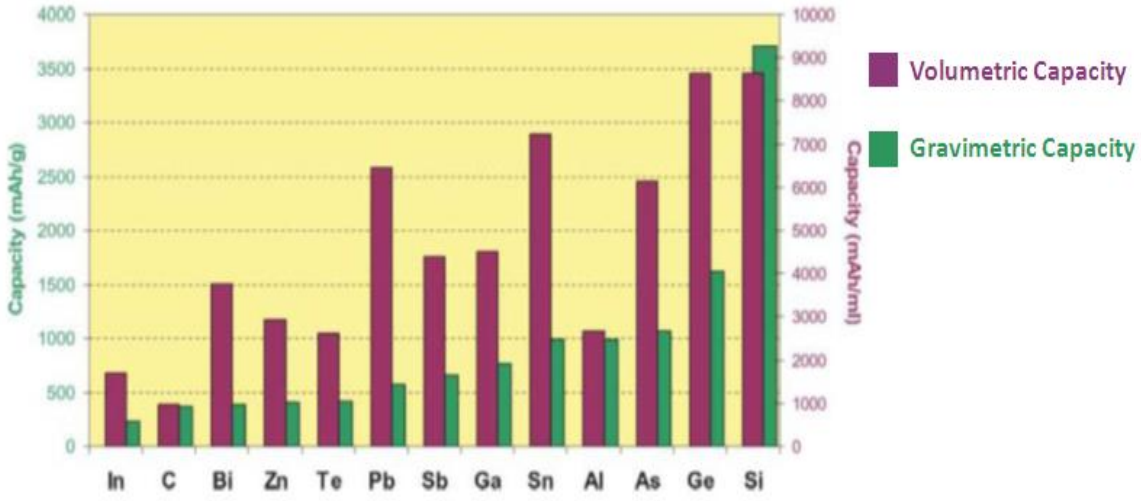

Figure 1.2. Gravimetric and volumetric capacities for selected alloying reactions [29]

Due to the relatively low capacity of the commonly used anode graphite, silicon has a huge advantage over the graphite as the candidate electrode. However, silicon anodes have their own limitations, because silicon thin films tend to crack and have volume changes during the insertion and extraction of lithium [30]. Additionally, silicon and lithium forms alloys such as $Li_{12}Si_7$, Li_7Si_3, $Li_{13}Si_4$ and $Li_{17}Si_5$ [31]. This process can cause volume of Si to expand as much as four times its original dimension [32-33]. These effect cause capacity

to fade dramatically after several hundred cycles. Figure 1.3 demonstrate a typical life cycle of a silicon thin film anode [34].

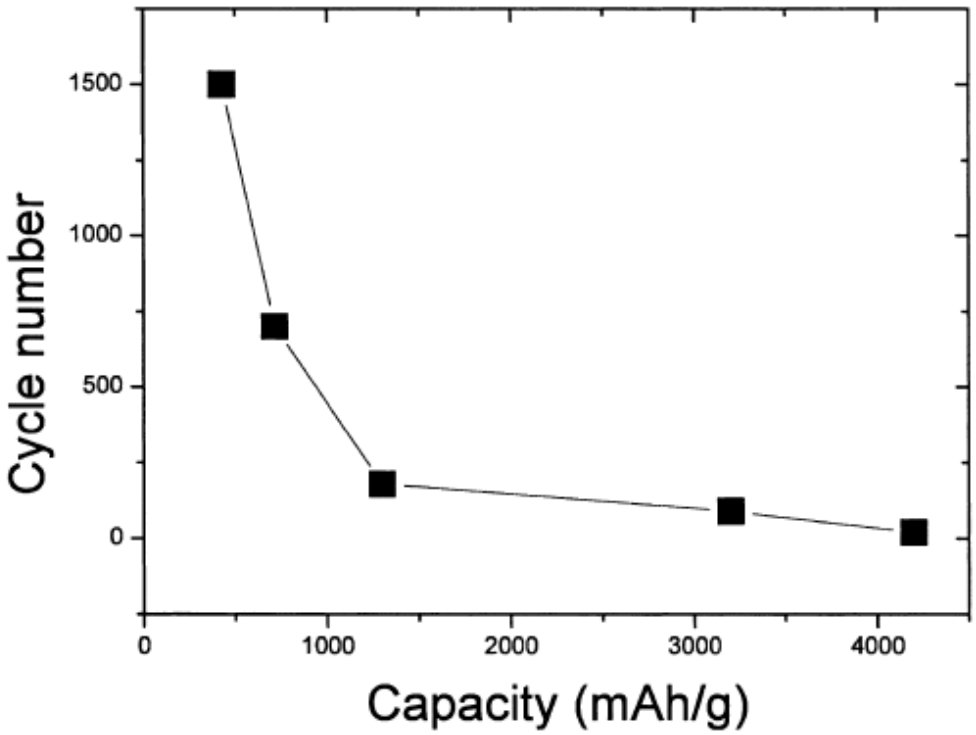

Figure 1.3. Cycle performance of a 0.5 micron silicon thin film anode [34]

Several methods have been applied to reduce the volume expansion problems with Si anode, including adding conductive materials, binders, surface modification, and introducing nanostructures.

Binders and conductive additive powders can be added to the electrode to improve battery capacity. Li [35] investigated using sodium carboxymethyl cellulose(CMC) which is an extremely stiff and brittle polymer as binder to Si (325 mesh size) powder can vastly improve cycling performance.

The use of surface modifications is another technique to improve cell capacity. Fu [36] showed that modification of the surface structures via either mild oxidation, deposition of metals or metal oxides, coating with polymers or other kinds of carbons greatly enhanced electrochemical performance.

Reducing the thickness of silicon thin films is another way to control the volume expansion and cracking, while retaining some of the capacity benefits of Si electrodes. The work by Maranchi, et al., [37] shows that thin film of 250nm Si deposited on copper foil yield capacities close to 3500mAh/g for 30 cycles employing a C/2.5 rate, while thicker one micron film exhibit about 3000mAh/g after 12 cycles.

Nanostructured electrodes are yet another promising way to improve cell capacity, cycling performance, and overall battery life. Lots of nanostructured electrodes have been investigated, including nanowires, nanoparticles, and nano-patterned electrodes [38-40]. Yi Cui's group from Stanford demonstrated that silicon anodes can maintain a discharge capacity close to 75% of its maximum using silicon nanowires [38], and later showed that active silicon nanotube anodes can cycle over 6,000 times in half cells while retaining more than 85% of their initial capacity [41]. Nanostructures provide the benefits of demonstrating a higher degree of strain relaxation and enhanced power rates. Due to their one dimensionality, nanowire electrodes can accommodate large strain without pulverization. Another approach involves mixing two or more materials to mitigate volume change. Mao [42] investigated alloyed Sn-Fe(-C) powders as battery anodes of 800mAh/g capacity, which is a great improvement over tin oxide composites in the cycling response. SnO based glasses have been investigated by Idota as potential lithium ion battery anodes.

They found that the SnO anodes yielded a specific capacity more than 50 percent higher than that of traditional carbon-based electrodes. [43]

1.4 Previous Works on Strain Development Within Lithium Battery Electrodes

Quantifying the mechanical deformations associated with lithiation/delithiation is critical for optimal battery performance and lifetime design, but direct measurement of anode mechanical deformations that accompany electrical cycling of lithium ion battery systems is challenging. Nearly all other previous studies attempting to measure *in situ* anode deformations have employed optically-based methods for observing the anode electrode inside a custom battery arrangement.

Most recently, V. Sethuraman, *et al*., [44-45] analyzed a silicon thin film anode system by using a laser optical detection method to determine *in situ* stress and mechanical property changes during charging/discharging. *In situ* mechanical stress evaluation for Ni-Sn alloy anodes was performed by Chen, *et al*., [46] using another laser measurement technique. In a similar way, Qi and Harris [47] used a custom battery fixture to observe deformation and cracking of a graphite electrode. In that study, the graphite deformation was determined using digital image correlation (DIC). Other uses of DIC includes a study by Okman, Jones, *et al*.,[48] in which cracking and self-healing of lithium ion battery electrodes was investigated, showing the mechanical effects binders and additives had on electrochemical performance. A nanostructured form of silicon was introduced by researchers to reduce large volume change and reduce capacity retention [49]. Carbon nanotubes are becoming widely integrated as a new material within lithium ion battery electrodes. Recent works have explored the use of aligned carbon nanotubes, which

showed no significant capacity degradation after 50 cycles [50]. A new carbon nanotube-silicon hybrid film for anode of lithium ion battery has been introduced in Stanford University, which showed a high specific capacity, while at the same time releasing the strains associated with large volumetric change [51]. Lithium-induced strain is a significant factor for generating high stress, capacity loss, crack and fracture within battery electrodes. Zhang *et al.* [52] demonstrated that nanowires embedded within carbon, aluminum or copper coatings significantly reduced radial expansion and tensile stress, and also improved electronic conduction.

1.5 Role of Substrate Adhesion on Electrode Degradation

During battery cycling, lithium ions diffuse into and out of anode materials, causing large volume change. Large volume expansions and contractions in anode films can cause significant cracking, capacity loss, degradation or failure. The adhesion between electrode and substrate also plays a number of significant roles in battery performance. The quality of adhesion with the substrate will often dictate whether the electrochemically-induced strains within the electrode materials are sufficient to cause failure/cracking. In addition, the adhesion quality between electrode and substrate (which serves as the current collector) will also influence the contact resistance and, thus electrical efficiency, of the system.

Surface treatment of copper substrate has been used to improve the adhesion through many different manners. [53-59] Surface modification could create anchor points for the electrode materials, so the electrode materials can better attach to the substrates. So even if the electrode materials got cracks, the electrical contact between electrode and substrate can be maintained.

Researchers also found that the formation of amorphous silicon-copper phases can lead to the weakening of interfacial adhesion between silicon and copper. So they proposed a nano-compliant support (NCL) layer between silicon film and copper substrate. And this NCL layer provides a highly compliant support structure which can relieve the stress between silicon and copper layer. [60]

Even though amorphous silicon deposited on copper substrate can reach near theoretical capacity within the first several cycles. The capacity will dramatically drop after 20-30 cycles depending on the film thickness.[61] The interfacial fracture energy of amorphous silicon on copper foil was determined by *in-situ* SEM tensile testing method which is proposed by Ignat.[62]

Some of the motivating previous works illustrate the issues at play during electrochemical cycling. Figure 1.4 shows silicon lithiation schematically in lithium ion battery. Figure 1.5 shows that significant lateral and vertical expansion of the initial silicon structure occurs during battery cycling. Figure 1.6 shows amorphous silicon thin film anode cracks under battery cycling.

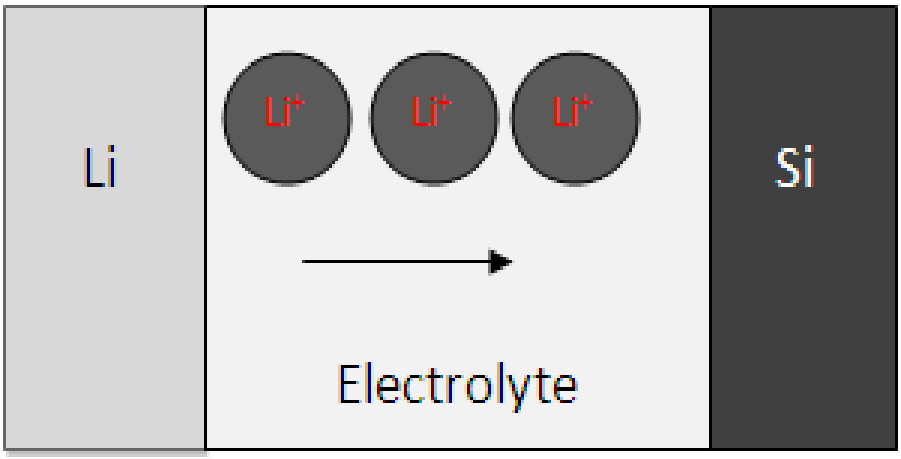

Figure 1.4. Silicon lithiation schematic

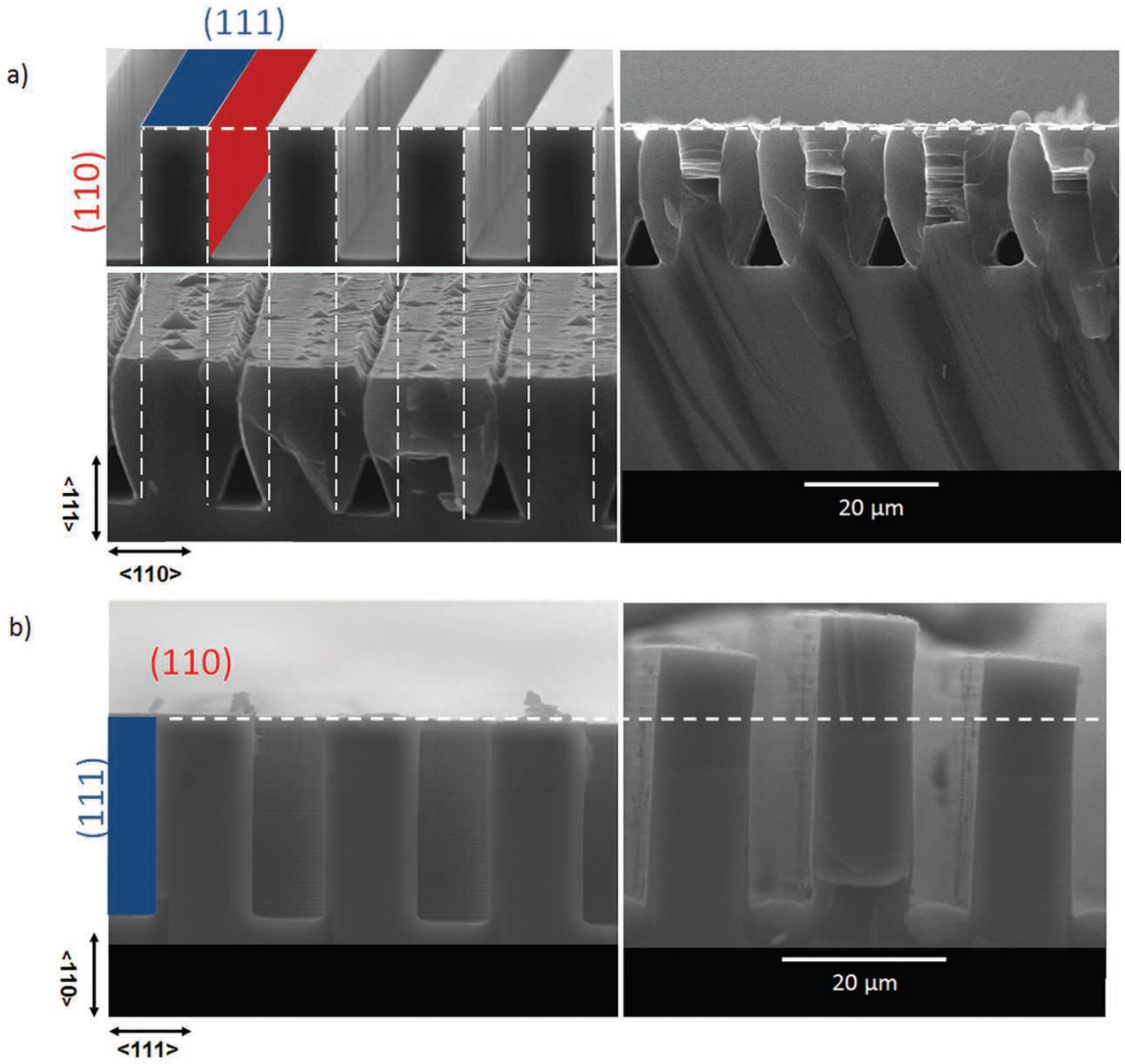

Figure 1.5. SEM cross sectional image for silicon wafer after galvanostatic charging [63]

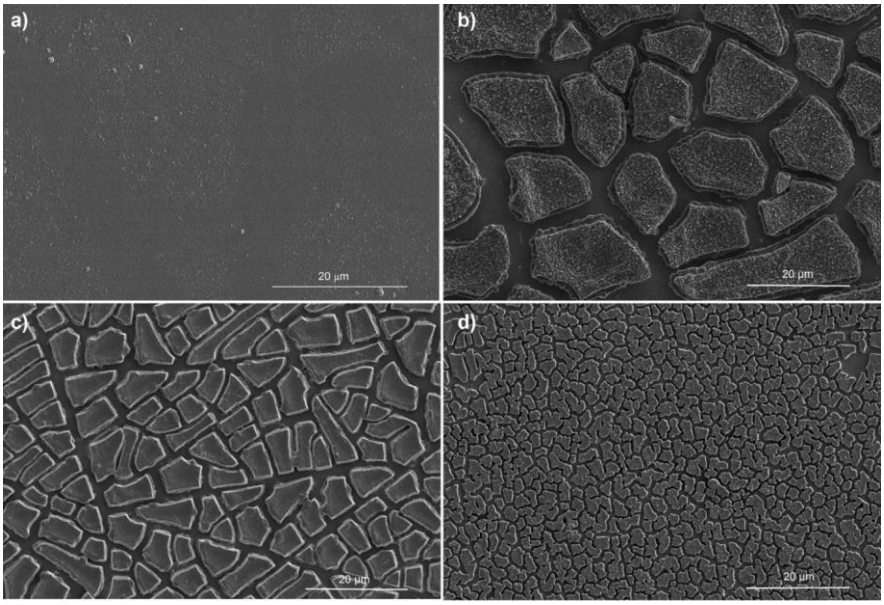

Figure 1.6. SEM images of silicon thin film before and after cycling [64]

1.6 Outline of Work Performed in This Study

Many battery performance characteristics are significantly influenced by the mechanical behavior of the materials/structures, and better understanding of this relationship can help mold future battery designs. This work strives to elucidate the mechanics connection between electrode, substrate, and electrical performance, specifically the roles of constraint and adhesion during lithium battery electrical cycling. To investigate the role of substrate mechanical interactions with electrode materials, *in-situ* measurement of electrode deformation during battery cycling using digital image correlation and experimental measurement of electrode-substrate adhesion using both laser spallation and double cantilever beam delamination tests are performed. This work also quantified the effects of substrate constraint and adhesion on lithium battery performance through the use of both

mechanical and battery cycling tests, with the overriding goal of helping future battery designers determine best practices and considerations for optimizing power and lifetime performance. Within this work, Chapter 2 will focus on the materials, procedures, and testing equipment used to quantify these effects. Chapter 3 will focus on the in situ testing of strain development and relation to substrate constraint, while Chapter 4 will investigate the role of substrate-electrode adhesion. Finally, Chapter 5 will discuss the conclusions that can be drawn from this study and suggestions for future work in the area.

CHAPTER II

EXPERIMENTAL TESTING TECHNIQUES

In this chapter, several experimental testing techniques are introduced that are widely used throughout the dissertation. These techniques include electrical cycling testing of lithium batteries, the digital image correlation measurement method, and laser spallation adhesion testing.

2.1 Electrical Cycling of Lithium Battery

One technique widely used to evaluate electrochemical performance is lithium ion battery charge-discharge testing. To properly analyze the performance of a lithium ion battery, it is necessary to understand cyclic voltammetry and galvanostatic cycling.

Cyclic voltammetry, or CV, is a commonly used electrochemical method to determine diffusion coefficients and half-cell reduction potentials. In a CV experiment, the electrode potential ramps linearly versus time. After the potential reach the peak, the potential is driven back to the initial value linearly. This cycle is repeated until the total number of test cycles has been completed. Figure 2.1 shows a typical cyclic voltammetry waveform during cell testing, [65] while Figure 2.2 shows the current at the working electrode versus applied voltage. [66]

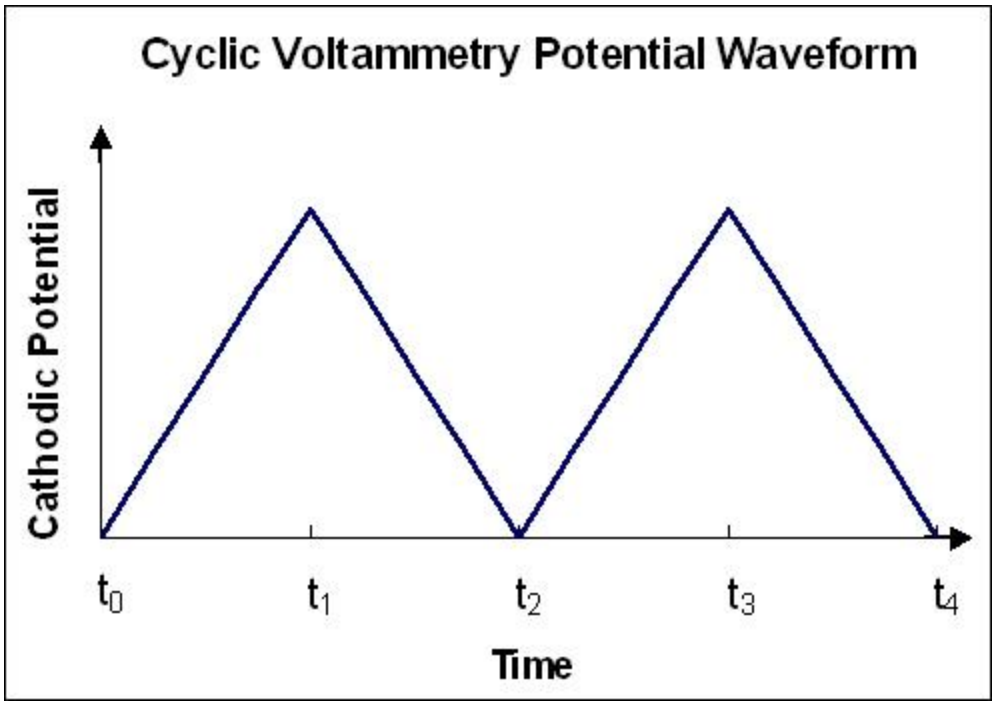

Figure 2.1. Cyclic voltammetry waveform [65]

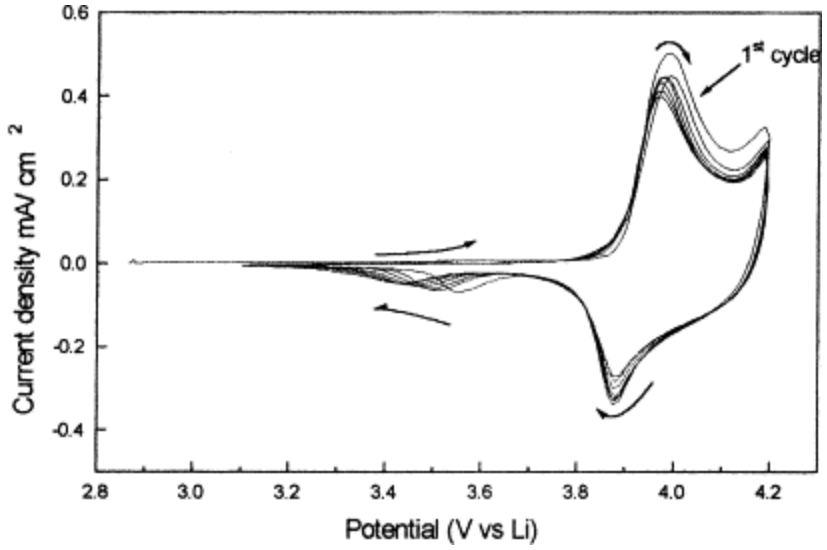

Figure 2.2. Cyclic voltammetry of a $LiCoO_2$ electrode in an EC-DMC electrolyte [66]

Galvanostatic cycling provides charging and discharging profiles for lithium ion battery. In galvanostatic cycling test, the coin cell is controlled at a constant current during the charging and discharging process.

Cyclic voltammetry is an important electrochemical technique to investigate the chemical reaction types as battery capacity fades. While in galvanostatic cycling, we can gather the information about the rate performance, structure of the intermetallics during lithiation and cycle lifetime of the lithium ion battery.

There usually are upper and lower voltage limits during these tests to compare. For the commonly used coin cell battery, a 2-3 volt upper limit and 0.02-0.05 volt lower limits are usually applied. The upper and lower limit is set constant to make to battery performance compare more meaningful.

2.2 Digital Image Correlation Measurements

Developed originally in the 1980s by Sutton and his colleague [67], digital image correlation (DIC) uses numerical algorithms performed on digitally recorded images taken of a specimen surface during an applied loading. Figure 2.3 shows typical types of digital images used in the DIC process before and after an applied deformation. The outputs of a DIC experiment are the surface displacements and strains over the full imaged field (in-plane for 2D versions). Given the difficulties presented by the experimental measurements of anode strain development, DIC offers several advantageous aspects. Some of these benefits include providing full-field displacement measurements and a non-contact measurement, allowing for a wide range of potential specimen dimensions. The components of a general 2D DIC experimental set-up are shown in Figure 2.4.

.

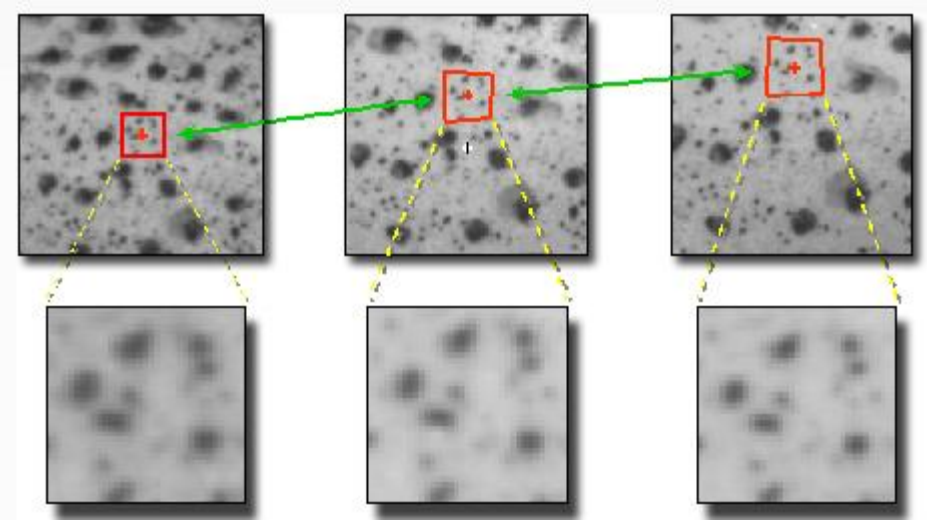

Figure 2.3. Images used in DIC before and after deformation [68]

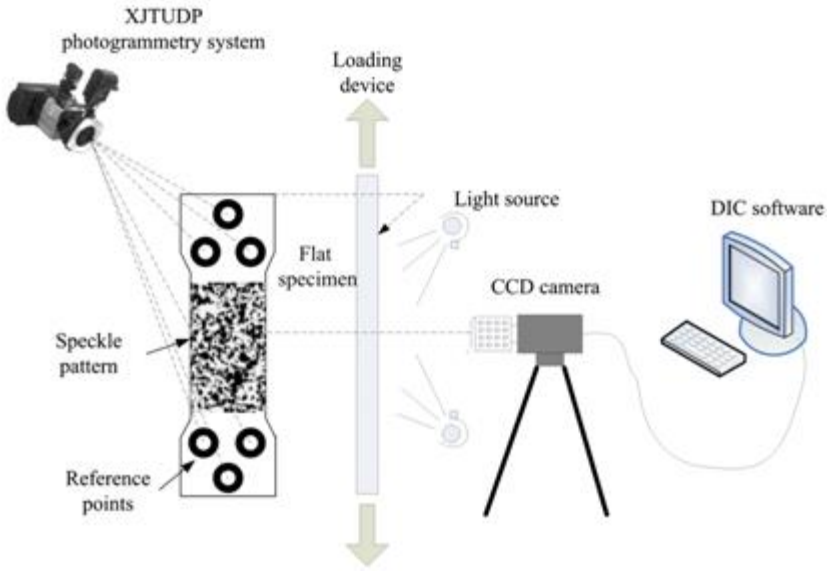

Figure 2.4. 2D-DIC schematic diagram [69]

2.3 Laser Spallation Adhesion Tests

Thin films are used widely in a number of commercial engineering fields, such as electronics, semiconductors, MEMS devices, and so on. Since thin films are usually less than one micron and can be as small as 10-100 nm, a substrate is required for deposition and support. Due to the large interfacial area compared to other geometrical dimensions at this size scale, the adhesion characteristics often dominate the overall mechanical response of the system.

There are several different mechanical adhesion measurements that can provide a characterization of adhesion strength, including the direct pull-off method, the ultrasonic method, a "scotch tape" method, and tangential shear method. However, it is difficult to get a quantified result from these kinds of tests, and the results can be skewed by the use of adhesive layers [70]. On the other hand, laser spallation tests can provide a repeatable and quantified measurement of the film adhesion using a technique that is non-contact based. As a result, the adhesion strength results using this method are much more accurate.

Laser spallation experimental testing was developed by Yuan and Gupta [71-73] to determine the tensile strength of thin film/substrate interfaces. In this method, a short (nanosecond scale), high energy laser pulse is shot from an yttrium aluminum garnet (YAG) laser. The laser pulse is directed through a transparent confining layer (usually water glass) to an absorbing layer (usually a very thin aluminum) on the backside of the substrate, with the thin film layer of interest on the front side of substrate, as shown in Figure 2.5. A rapid thermal expansion occurs due to laser energy absorption by the metal layer. The result is a compressive stress wave that travels through the thickness of substrate. The stress wave

propagates towards the film-substrate interface and then reflects from the free film surface as a tensile wave, loading the testing interface in tension. A Michelson type interferometer is used to measure the displacements at the free film surface. The magnitude of the stress pulse of the film-substrate interface is proportional to the applied laser power and the mass of the film layer. So, we can determine the threshold of adhesion strength by incrementing the laser power and inspecting the sample surface for failure. If the interfacial stress is high enough, the reflected tensile pulse will induce delamination visible upon post-testing inspection of the film surface. A high resolution oscilloscope will be used to record the interferometric fringes corresponding to substrate displacement, characterizing the baseline substrate stress profile as a function of laser power. Figure 28 shows a schematic of tensile laser spallation technique components [74] and Figure 2.6 shows the actual experimental setting in our lab.

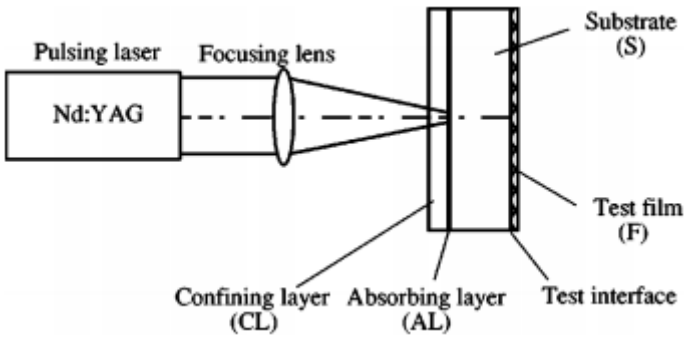

Figure 2.5. Schematic of tensile laser spallation technique [74]

Figure 2.6. Experimental set-up of laser spallation system

CHAPTER III

EFFECTS OF SUBSTRATE CONSTRAINT ON IN-SITU STRAIN DEVELOPMENT WITHIN LITHIUM BATTERY WORKING ELECTRODES

Lithium batteries are fabricated based on a modification of the standard CR2032 coin cell configuration. The custom cell allows optical imaging of the anode throughout the process of battery cycling. The steps for producing and testing these cells are included in the following subsections. (Part of results of this chapter have been published. Reprint permitted, Chen. et al. Journal of Power Sources, 271, Dec. 2014, 406-413)

3.1 Specimen Preparation

For electrochemical and *in-situ* strain testing, three different anode materials were investigated: amorphous silicon, traditional graphite, and a carbon nanotube-based composite. These specimens were prepared on different substrates, as detailed below.

3.1.1 Working Electrode Materials

Amorphous Si thin films were deposited by RF magnetron sputtering onto a 635μm thick flat copper disk or 16 micron thickness copper foil (Technics 4604 Sputter Coating System) which is shown in Figure 3.1. A four inch diameter round target of pure Si (99.99%, Kurt J. Lesker) is used for the sputtering deposition. A 5 minute pre sputtering procedure was used to remove any native silicon dioxide before the final sputtering. Si thin films were deposited by a 300W RF power supply for a duration typically between 30 minutes and 60

minutes, depending on the desired thickness. During deposition, the chamber pressure was set at 25 mTorr with Argon flowing as the process gas. Film thickness was measured by (Veeco Dektak 8M profilometer) to be 500 nm to 1000 nm.

Figure 3.1. Technics 4604 Sputter Coating System used for silicon film deposition

Graphite-based thick films (10 µm) deposited on copper substrates were used as the anodes within the custom coin cell batteries. In addition, the effects of using conductive carbon nanotubes (CNTs) as graphite replacement were studied.

Graphite anodes were prepared by mixing 80 wt% graphite powder, 10 wt% carbon black, and 10 wt% polyvinylidene fluoride (PVDF) binders in N-Methyl-2-pyrrolidone (NMP) solvent. The well-mixed slurry was deposited over the copper substrate, and a film casting doctor blade apparatus was used to skim the wet electrode to a thickness of 10 microns. The electrode and substrate were then immediately put into a laboratory oven at 115ºC for 15 minutes.

Specimens containing the conductive CNTs as a graphite replacement were prepared in a similar manner. The CNTs used in this study were purchased in bulk commercially (Cheaptubes.com) and had diameters in a range of 60-80 nm and lengths in the range of 10-15 μm. The 80 wt% CNTs were first combined with 10 wt% carbon black and blended in an industrial mixer a period of 12 hours. Next, 10 wt% PVDF binder and NMP solvents were injected into the mixture, which was then blended for an additional 12 hours. The slurry was then cast onto the copper substrates, skimmed to the proper thickness, and finally oven cured at 115ºC for 15 minutes.

3.1.2 Substrates

To investigate the effects of substrate constraint, two types of copper substrates were tested, 16 μm thick copper foils and 635 μm thick copper disks. Both were purchased commercially from Grainger Engineering Supply, Inc. The electrodes and substrates combination tested in the experiments are shown in table 3.1.

Table 3.1.

Electrodes and substrates combination tested

Battery Sample Type	Electrode material (Thickness)	Substrate (thickness)
1	a-Si (1μm)	Copper Disk (635μm)
2	Graphite (10μm)	Copper Foil (16μm)
3	Graphite (10μm)	Copper Disk (635μm)
4	CNT-Based Composite (10μm)	Copper Foil (16μm)
5	CNT-Based Composite (10μm)	Copper Disk (635μm)

3.1.3 Custom Coin Cell Assembly

To allow optical access to the working electrode, a 6.35 mm diameter through-hole was first placed through the center of the coin cell cover cap using a mechanical punch. A 12 mm diameter round, 0.15mm thick glass cover slip (Ted Pella) was bonded to the top surface of the cell cap by applying CRL 349 ultraviolet adhesive (Loctite Impruv), followed by a two minutes UV exposure cure. This top cover was found to be sufficient to seal the coin cell, but necessitated a custom fixture during crimping to prevent damage to the glass window.

The custom CR2032 coin cell was assembled in an Argon filled glove box (Figure 3.2). All parts, including cell cap, gasket, spring (Hohsen), and glass fiber separator (Advantec) were put into a 80°C heated chamber (Buchi glass oven B585) and connected to a vacuum pump for eight hours to completely remove water moisture and evaporated solvent prior to assembly. For all coin cell configurations, a pure lithium metal disk (Sigma Aldrich) was used as the counter electrode. Additional through-holes, approximately 6 mm in diameter, were created in both the lithium metal electrode and the separator while housed under the assembly glove box using a gasket punch.

An electrolyte consisting of 1M LiPF6-EC:DMC (1:2 by volume) was used throughout this work, with ca. 0.5 mL volume used for each cell. After stacking the layers and adding the electrolyte, a hand-operated crimping tool (Hohsen) was used to close and seal the coin cell batteries. A schematic showing the individual coin cell layers and an actual completed coin cell after assembly are shown in Figure 3.3.

Figure 3.2. Argon filled glove box used for coin cell assembly

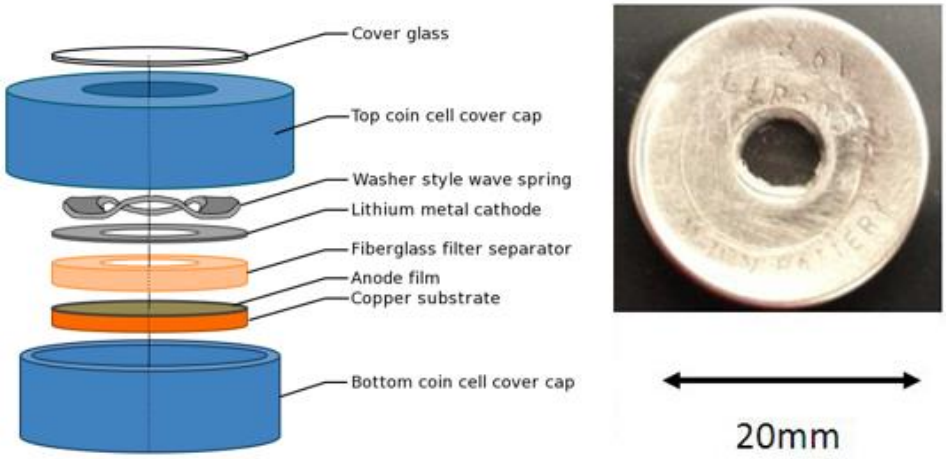

Figure 3.3. Coin cell structure diagram (left) and a typical actual coin cell (right)

3.2 In-Situ Strain DIC Results during Electrical Cycling

Electrochemical characterization of the custom CR-2032 coin-type cell performance was conducted in an Arbin BT2000 battery tester (Figure 3.4). Immediately after fabrication, the coin cell batteries were electrically cycled while the images were simultaneously taken of the anode surface.

3.2.1 Test Conditions

As fabricated batteries were first discharged under 0.1mA constant current conditions until a cut-off voltage of 0.020V was reached. After a 30 second rest period, a constant current of 0.1 mA was applied to cell during the charging cycles until the battery high potential cut-off was reached, which was 3V for the graphite anodes and 2V for silicon and the CNT anode systems. After a 30 seconds rest period, a 3V constant voltage charge for graphite or a 2V constant voltage charge for silicon and CNT anode systems was applied to the battery for 5 seconds. After a 10 sec. cool down, the next discharge cycle was begun. This process was repeated for approximately 20 cycles using the same loading conditions. This electrochemical characterization procedure is shown schematically in Figure 3.5.

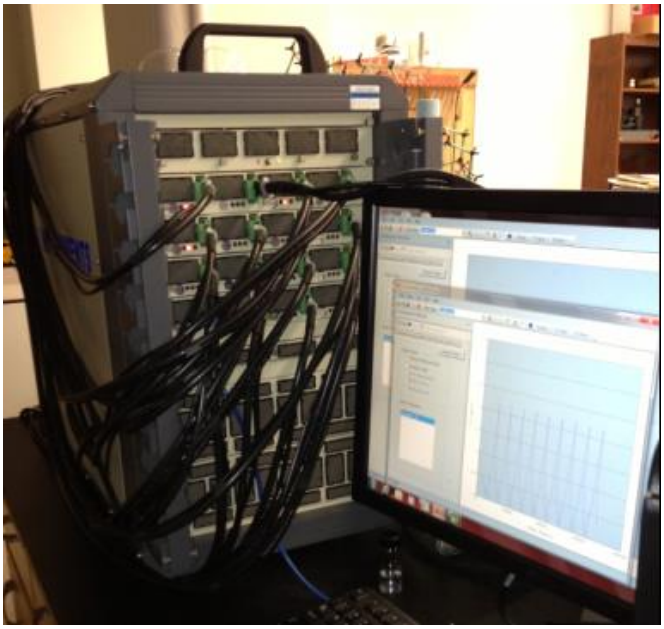

Figure 3.4. Arbin instrument BT2000 battery test station

Figure 3.5. Electrochemical characterization during battery cycling

3.2.2 DIC Results with Amorphous Silicon Thin Film as Working Electrodes

During the battery cycling, a Leica DMR microscope mounted with a Retiga 4000R digital camera from QImaging (2048 x 2048 pixels) was used to capture images of silicon thin film electrode surface through the coin cell window, Figure 3.6. A series of images were taken before and after discharge/charge cycles, and a 10X long working distance objective is used to capture the images.

The inherent surface roughness of the substrate was found to provide a suitable pattern for performing digital image correlation. An in-house written DIC algorithm was used to calculate the average bi-axial in-plane strain within the anode films. Strains were computed in the plane of the anode surface by differentiating the displacement fields found. These measurements were performed in both the vertical and horizontal directions (in the plane of the anode film), and average strain values were calculated in the middle of coin cell opening. Baseline measurements were used to quantify the noise in the measurements, with baseline displacement resolution for individual subsets determined to be approximately 1/10th of a pixel.

Typical electrode images before and after cycling are shown in Figure 3.7.

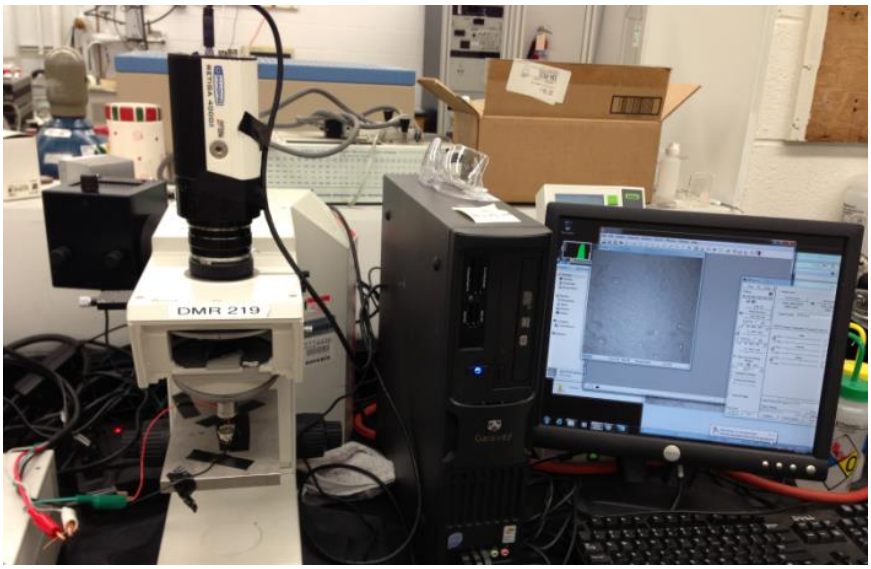

Figure 3.6. Leica DMR microscope mounted with a Retiga 4000R digital camera from Qimaging used to capture images

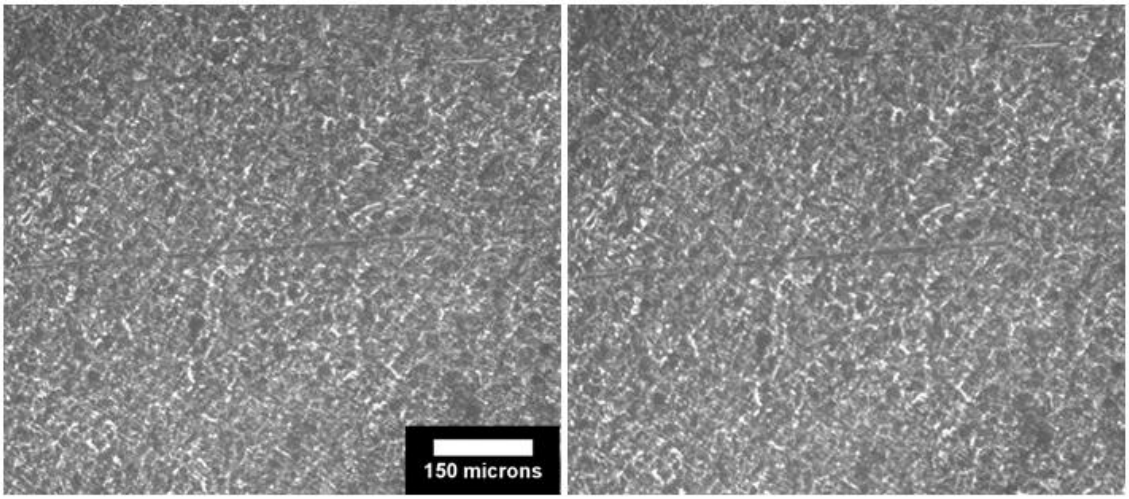

Figure 3.7. Silicon thin film images taken before (left) and after first discharge (right)

A digital image correlation analysis was performed on a number of the images taken of the silicon electrode surface. The most significant changes in the in-plane strain observed for the anode corresponded with images correlated between the fully charged and fully

discharged states. For the sample data shown in Figure 3.8, the largest observed strain differential occurred between states C and D with an average magnitude of 1.34 x 10^{-2}. Comparatively, strain measurements on the very first cycle (corresponding to states A and B in Figure 3.8) between the initial image of the "as fabricated" anode and an image at the time of the first complete discharge, yielded an average strain differential of around 5.0 x 10^{-3}. For both cases, the strains reported were found by differentiating the displacement fields. These values were averaged over the field of view in both the "x" and "y" directions, and compared favorably with the direct DIC computed strains. Figure 18 shows voltage and current curves during battery cycling, and overall discharge and charge capacities with respect to number applied cycles.

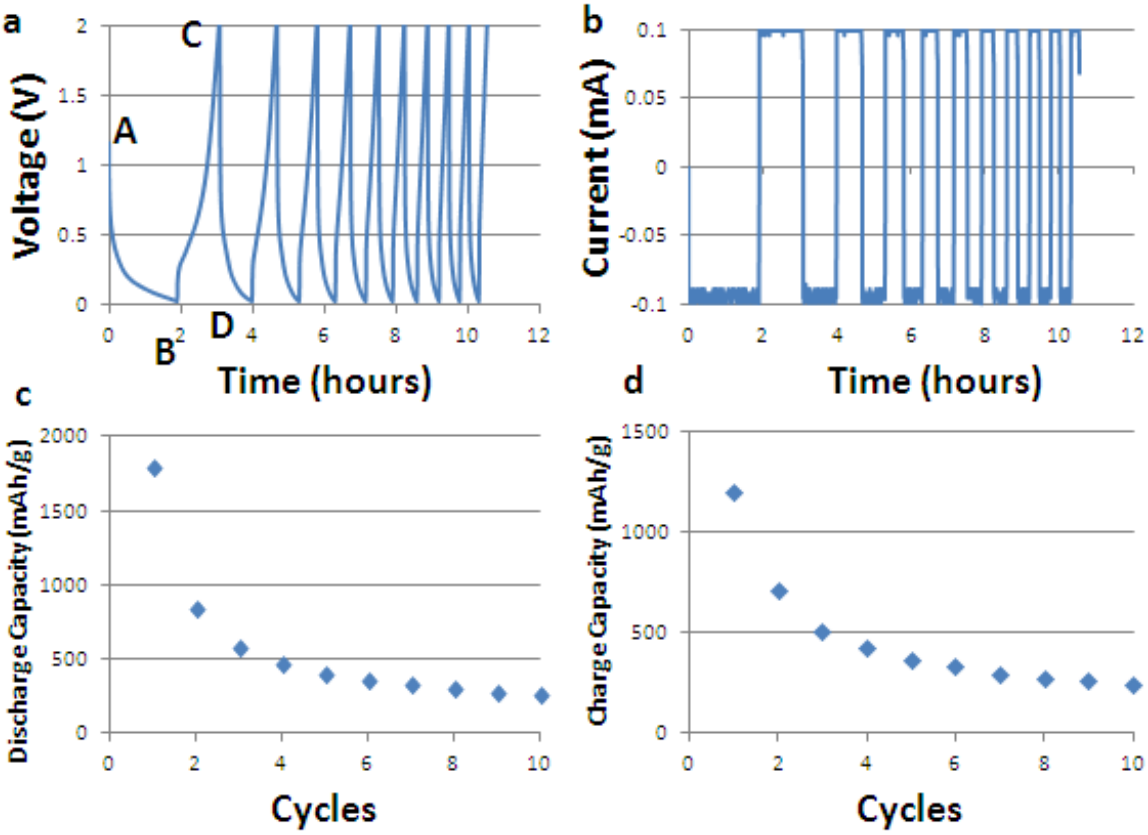

Figure 3.8. Voltage (a) and current curves (b) during the battery cycling, and the overall charge (c) and discharge (d) capacities with respect to number applied cycles.

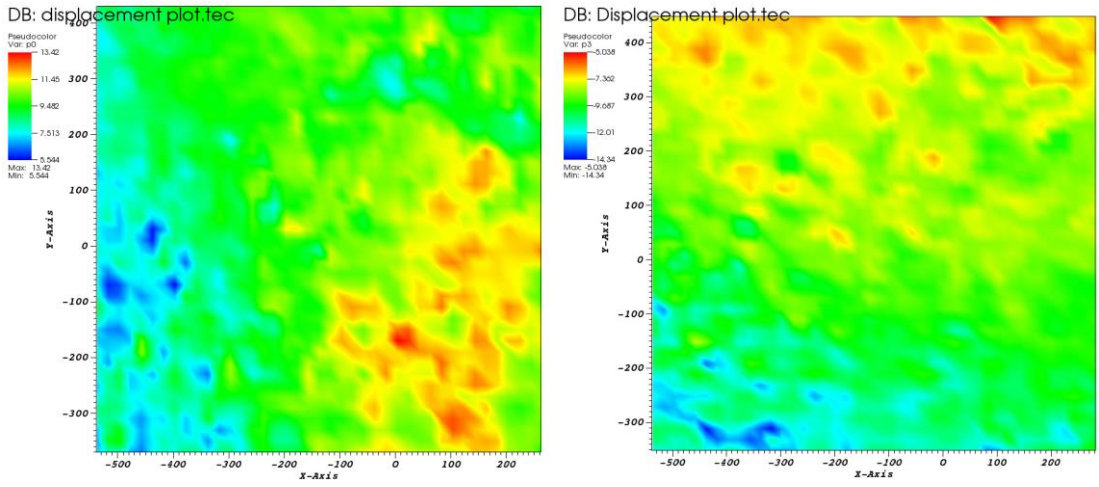

Figure 3.9. Displacement plot of DIC process in both "X" (left) and "Y" (right) direction

From Figure 3.9, we can clearly see the displacement gradients in both "X" and "Y" directions. And these displacement gradients will result tensile strain in both directions. The average strains in "X" direction are close to the strains in "Y" direction, giving confidence in our measurement.

Later in the battery lifetime, lower strains are expected as anode cracking begins and less volumetric expansion occurs, which coincided with diminished capacity. Cracking of the thin amorphous silicon layer is likely driven by inadequate adhesion with the substrate. For certain silicon layer thicknesses and sputter coating deposition conditions (higher temperatures and rates), it was also observed that the residual film stresses that developed were sufficient to cause delamination. Current work in progress with regards to this area is examining the roles of adhesion and substrate compliance on the rate of capacity degradation.

3.2.3 DIC Results with Graphite and CNT as Working Electrodes

Prior to beginning the first electrical cycle, a reference image of the anode surface "as fabricated" in the sealed custom coin cell was taken which served as the baseline state for later deformation measurements during electrical cycling. Typical optical images of the anode surfaces are shown in Figure 3.10a and 3.10b, while the microstructures of both surfaces are shown in SEM images in Figure 3.10c and 3.10d.

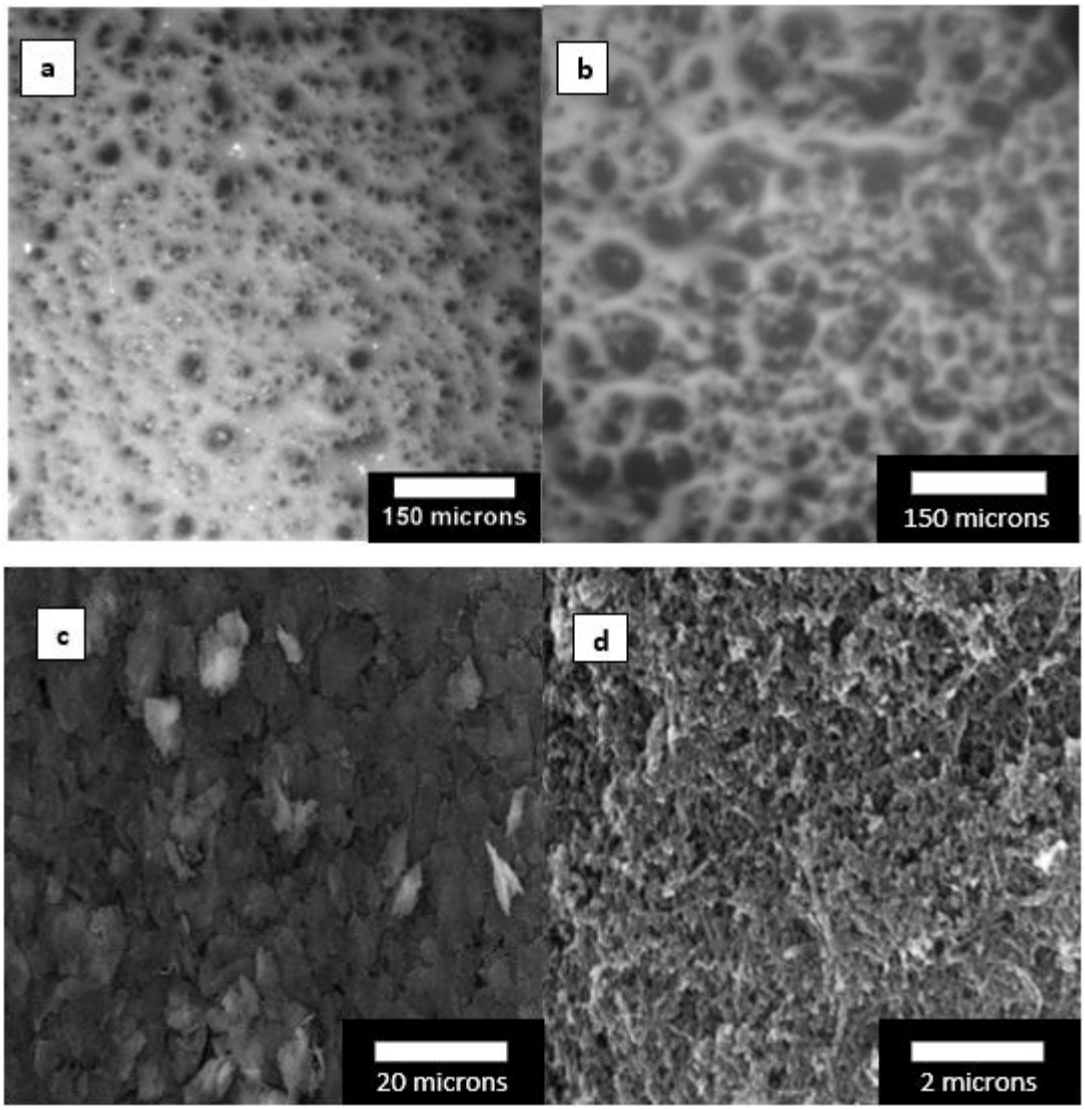

Figure 3.10. Optical microscope images of a typical graphite anode surface (a) and CNT-based anode surface (b) and SEM images of graphite (c) and CNT-based anode surface (d).

The effects of the anode/cathode surface area ratio on electrochemical performance were also considered. Son, *et al*., [75], examined these effects and found degraded coulombic efficiencies and discharge capacities for ratios greater than ~1.36. For this study, the same anode/cathode surface area ratio of ~1.13 was used for all specimens tested to minimize these effects. A number of control coin cell batteries without optical viewing windows (no

holes in cap, separator, or cathode) were fabricated and electrically cycled. These control specimens exhibited very similar overall performance, including initial discharge capacity and capacity degradation, as the custom coin cell batteries.

The results of electrical cycling and the corresponding strains measured via DIC for graphite anodes on foil and disk substrates are shown in Figure 3.11 and Figure 3.12, respectively. Average strains were found from differentiated displacement fields, and correspond to deformations that occurred with the imaged anode surface with respect to the "as fabricated" state (assumed to be undeformed). In both graphite anode cases, the maximum bi-axial tensile strains during each individual charge/discharge cycle were observed at the point of maximum discharge. For the lithium ion coin cell, the maximum discharge point is physically related to the state in which the graphite anode is saturated with lithium ions. Similar behavior was observed in results for the CNT-based anode specimens, shown for the foil case in Figure 3.13 and the disk case in Figure 3.14. The initial discharge capacities for all specimen types are shown in Table 3.2.

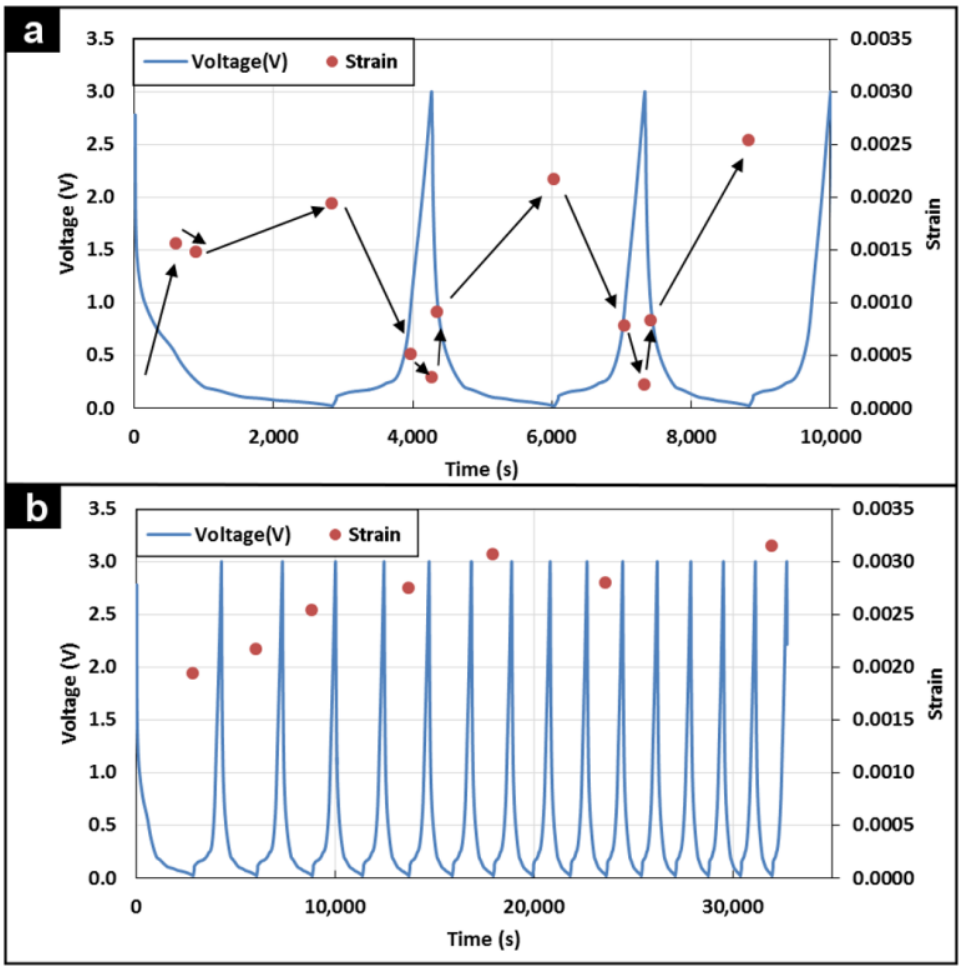

Figure 3.11. For a graphite anode with a copper foil substrate (16 μm), the electrical cycling and corresponding average anode strains calculated via DIC at multiple points for the first few cycles (a) and at the maximum discharge state only (b).

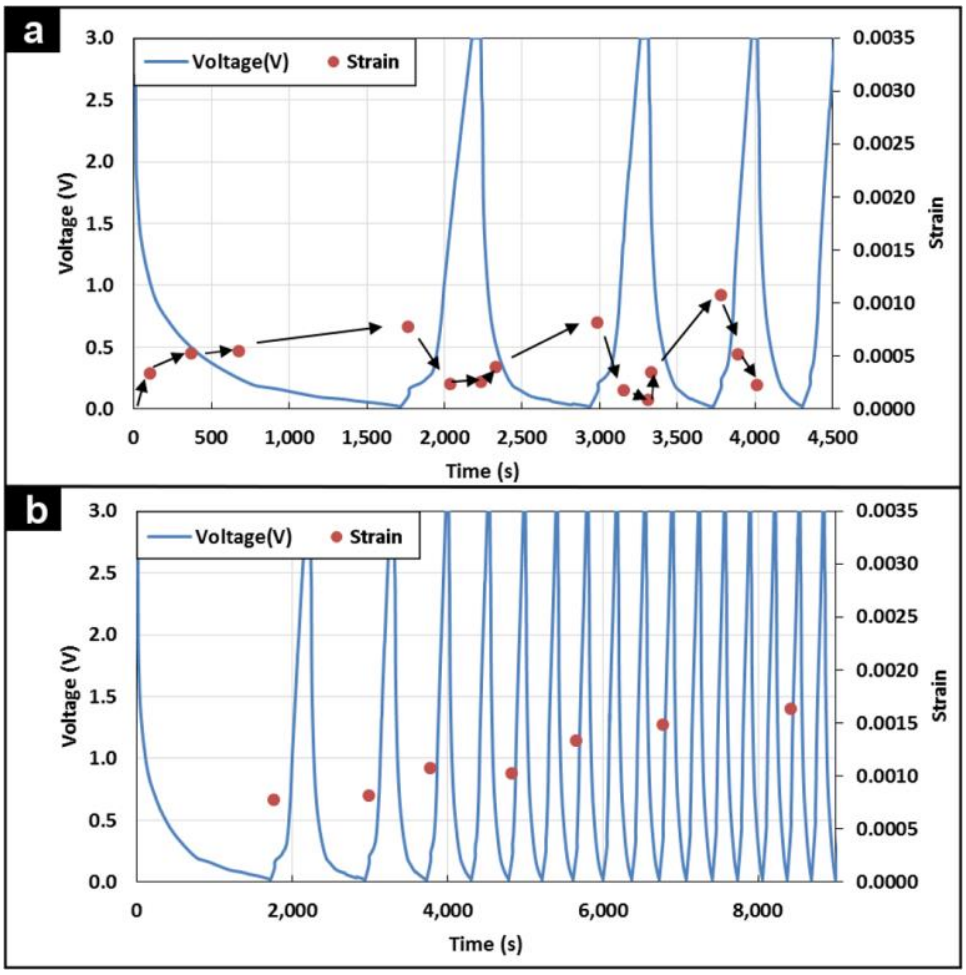

Figure 3.12. For a graphite anode with a copper disk substrate (635 μm), the electrical cycling and corresponding average anode strains calculated via DIC at multiple points for the first few cycles (a) and at the maximum discharge state only (b).

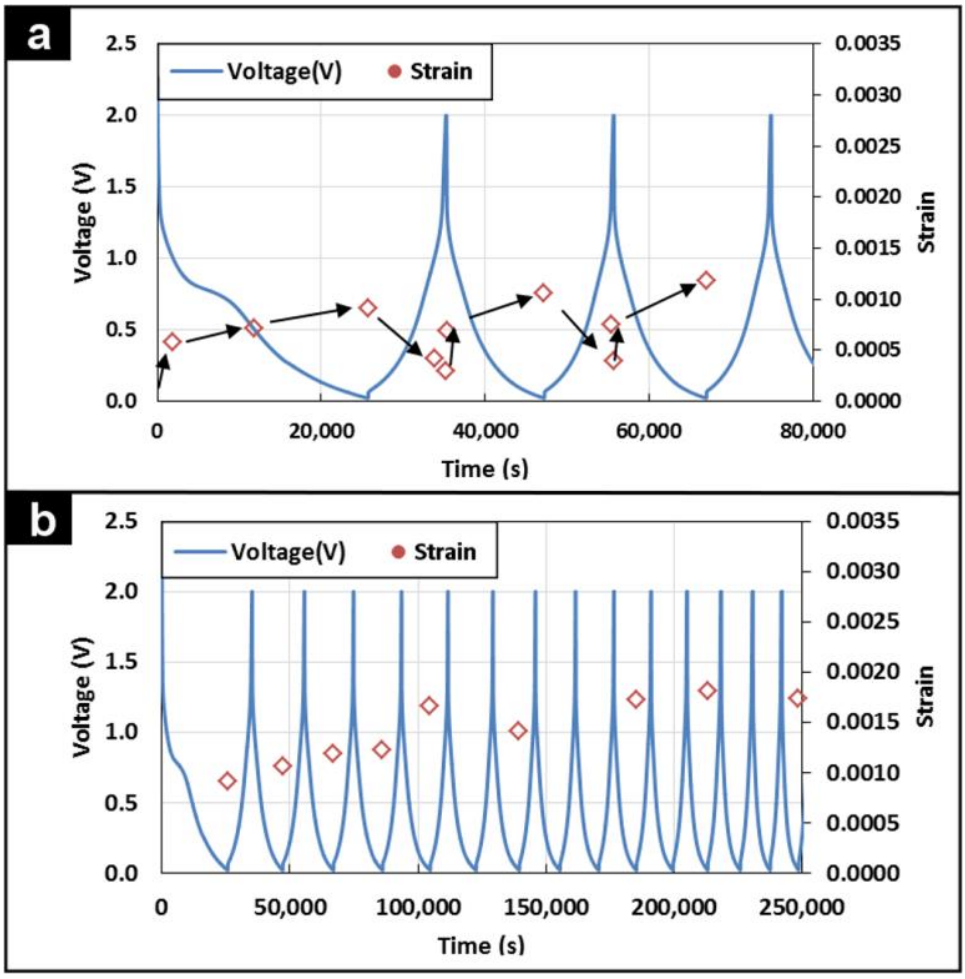

Figure 3.13. For a CNT-based anode with a copper foil substrate (16 μm), the electrical cycling and corresponding average anode strains calculated via DIC at multiple points for the first few cycles (a) and at the maximum discharge state only (b).

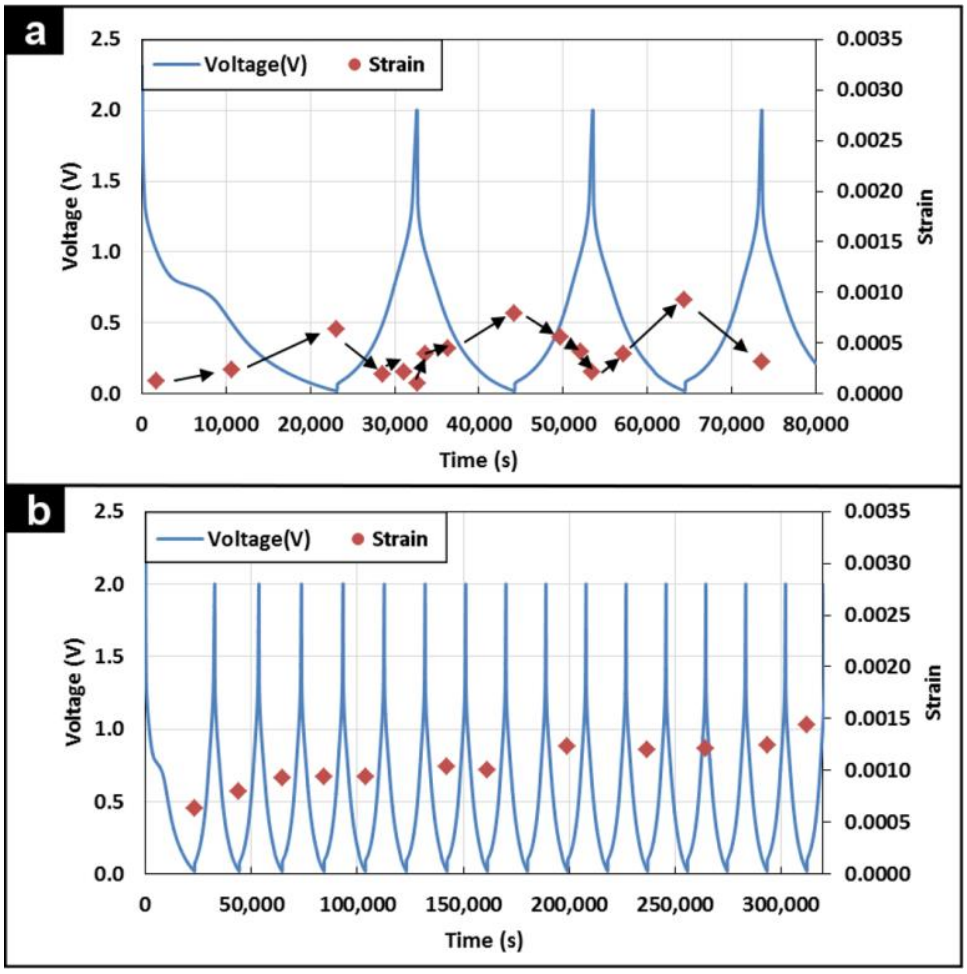

Figure 3.14. For a CNT-based anode with a copper disk substrate (635 μm), the electrical cycling and corresponding average anode strains calculated via DIC at multiple points for the first few cycles (a) and at the maximum discharge state only (b).

Table 3.2.

Initial Average Discharge Capacities

Anode Type	Initial Discharge Capacity (mAh)	Anode Mass (mg)	Specific Discharge Capacity (mAh/mg)
Graphite/Cu Foil	0.728	3.80	192
Graphite/Cu Disk	0.906	4.01	227
CNT/Cu Foil	1.360	4.30	316
CNT/Cu Disk	1.320	4.20	293

The strain magnitudes represent bi-axial in-plane deformations of the anode, which are greatly affected by the substrate constraint conditions. For both graphite and CNT-based electrodes, the strains within anodes deposited on copper foil substrates were significantly larger than strains measured for the copper disk substrate specimens; an expected effect due to the greater rigidity of the disk. In all cases, out-of-plane deformations likely occur, but appeared to be uniform over the field of view based on focal plane observations. Though not directly measured, greater out-of-plane deformations likely occur for the disk substrate batteries to reach comparable volumetric expansions, and thus electrical capacities, as the foil cases.

One of the most significant observations is that as the number of charge/discharge cycles increases, there is a continual increase in the residual strains within the anodes. In other words, to achieve the same potential charge at the end of each cycle, larger anode deformations are required as the cycle number grows. At the same time, battery capacity decreases as the number of cycles increase. These effects are summarized for the graphite

anodes in Figure 3.15, and for the CNT-based anodes in Figure 3.16. Comparing Figure 3.15 and Figure 3.16, the rate of discharge capacity degradation in the graphite anodes is much higher than that demonstrated by the CNT-based anodes. Although the induced bi-axial strains are higher in magnitude for the foil substrate cases, the rate at which the induced strains change with respect to cycle number did not vary much between the two substrate options.

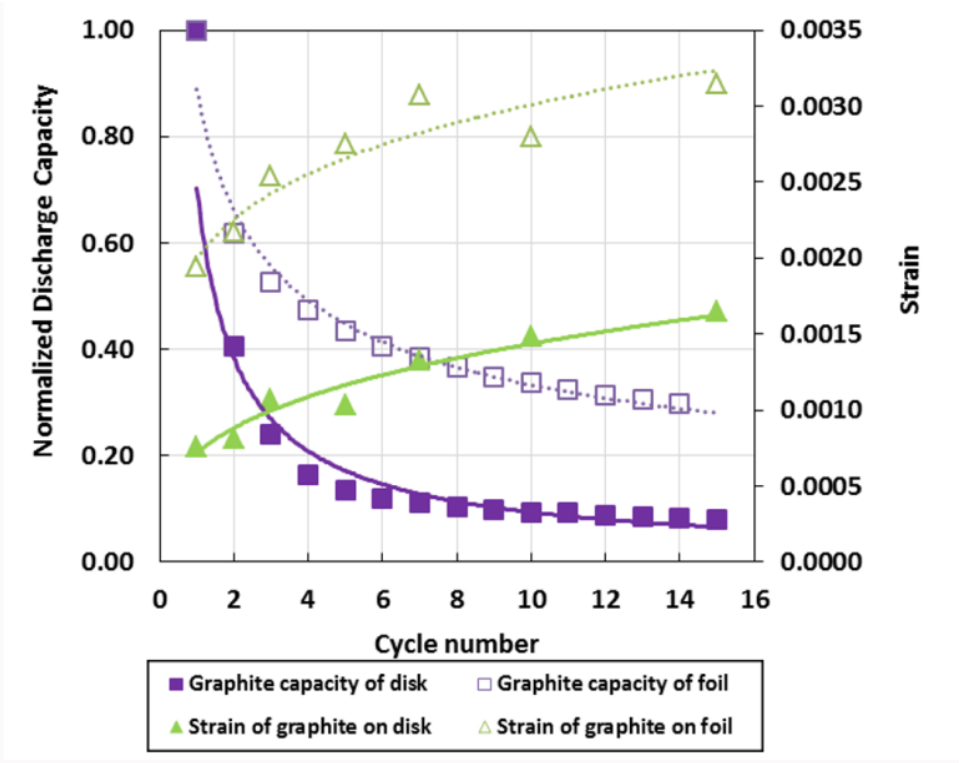

Figure 3.15. Normalized discharge capacity and corresponding anode strain for graphite anodes deposited on both copper foil and copper disk substrates are shown as the number of electrical charge/discharge cycles increases.

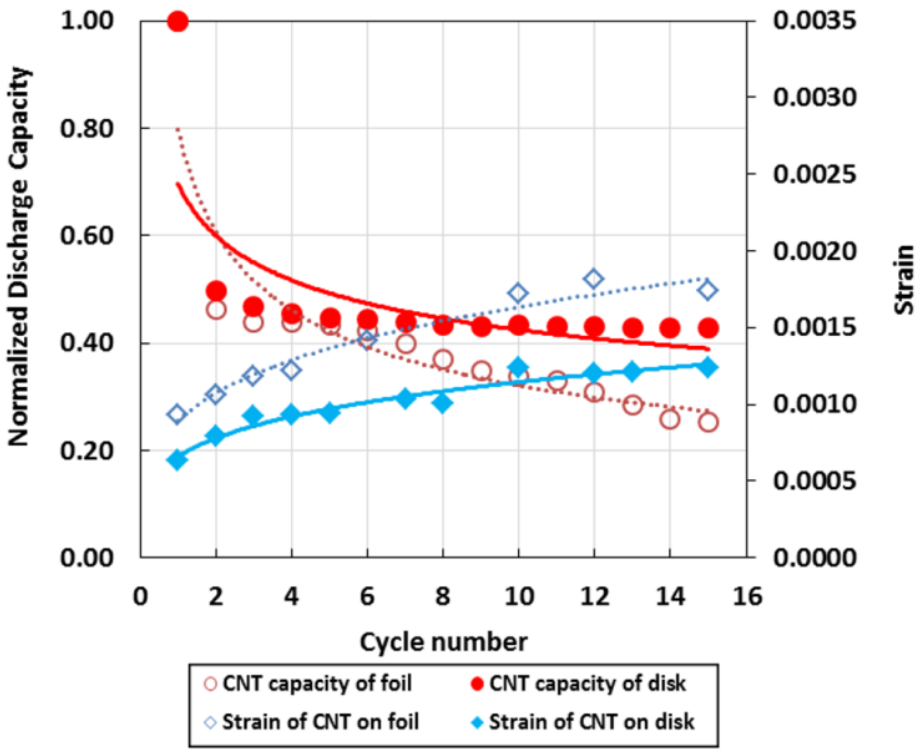

Figure 3.16. Normalized discharge capacity and corresponding anode strain for CNT-based anodes deposited on both copper foil and copper disk substrates are shown as the number of electrical charge/discharge cycles increases.

By comparing the results, substantial strains in CNTs are usually smaller than the strains in graphite electrode. For example, maximum strain in graphite electrode with copper foil substrate is 0.31%, while maximum strain is 0.17% in CNTs electrode which copper foil serve as substrate in both cases. Flexibility of the CNTs should be the main reason for the difference.

The relationship between SEI formation and the induced graphite anode strains was also explored through examination of the first electrical cycle, data for which is provided in Table 3.3. It is widely accepted that SEI formation occurs during the first electrical cycle

and is responsible for much of the irreversible capacity loss found for nearly every type of commercially viable Li-ion battery configuration. Novak, et al., [11] indicate that SEI formation occurs primarily in the 0.8V-0.2V regime during the first electrical cycle for graphite anodes. Over this potential range, SEI film formation did not appear to have a substantial mechanical effect. In fact, anode strains due to Li-ion intercalation seem to occur throughout the entire discharge cycle.

Table 3.3.

Graphite electrodes, First Cycle Strains

Anode Type	**3.0V-0.8V Δ Strain (% of 1st cycle total)**	**0.8V-0.2V Δ Strain (% of 1st cycle total)**	**0.2V-0.05V Δ Strain (% of 1st cycle total)**
Graphite/Cu Foil	0.00105 (54.1%)	0.000450 (23.2%)	0.000440 (22.7%)
Graphite/Cu Disk	0.000375 (48.4%)	0.000185 (23.9%)	0.000215 (27.7%)

In summary, as would be expected, the largest strain differential was observed to occur between the peak lithiation and delithiation states of the anode. It should be noted that the strain magnitudes measured represent in-plane deformations of the anode, which are greatly affected by the substrate constraint conditions. Significant out-of-plane deformations also likely occur, but appeared fairly uniform over the field of view.

Based on the experiment above, we found tensile strain occurs while battery is discharging and compressive strain occurs while battery is charging in the first several cycles. Graphite electrode lithiation causes the in-plane expansion while electrode delithiation leads to in-plane contraction. Substrate plays significant roles in strain development. Electrode strains with copper foil substrate are usually larger than strains with copper disk substrate.

At later cycles, the average strains measured dropped, but eventually became difficult to substantiate due to degradation of the anode material (cracking). This degradation of the anode material corresponded with reduced charge/discharge capacities and produced increasing changes in the surface appearance, giving a non-ideal pattern for DIC measurements.

3.3 ANSYS Modeling of Custom Coin Cell Electrical Field

In order to take the images of the electrode inside the customized CR2032 coin cell, holes in the separator, lithium metal and coin cell cover were required. So, it is necessary to investigate the effect of these openings in the middle of the cell. Compared to the normally operated CR2032 coin cell, the opening size of our customized cells is about 6mm in diameter and the electrode inside the cell is 18mm diameter.

A finite element analysis model was built with ANSYS to simulate the effect of the opening in these intermediate layers of the cell on electrical field. The results of ANSYS modeling for an electrical potential applied between the bottom and top electrode with a center opening portion removed are shown in Figure 3.17a. Three kinds of materials were used in the simulation, lithium metal electrode on top, silicon electrode on bottom and electrolyte in the middle. Material properties are: Silicon resistivity is 1000 Ωm, Lithium

resistivity is 92.8E-9 Ωm. Relative permittivity of Silicon, Lithium and electrolyte is 11.68, 40 and 37, respectively.

Constant voltage of 3V is applied on top of lithium metal layer and grounded at silicon layer; electric field distribution in radial direction is shown in Figure 3.17. Of particular interest was the possible creation of electrical field gradients on the anode surface in the regions imaged in the experimental DIC analysis. On the anode surface, the only non-uniformities in the potential field found to exist were located beneath the inner edge of the cathode, Figure 3.17b. Otherwise, the center of the anode experiences a nearly uniform potential field.

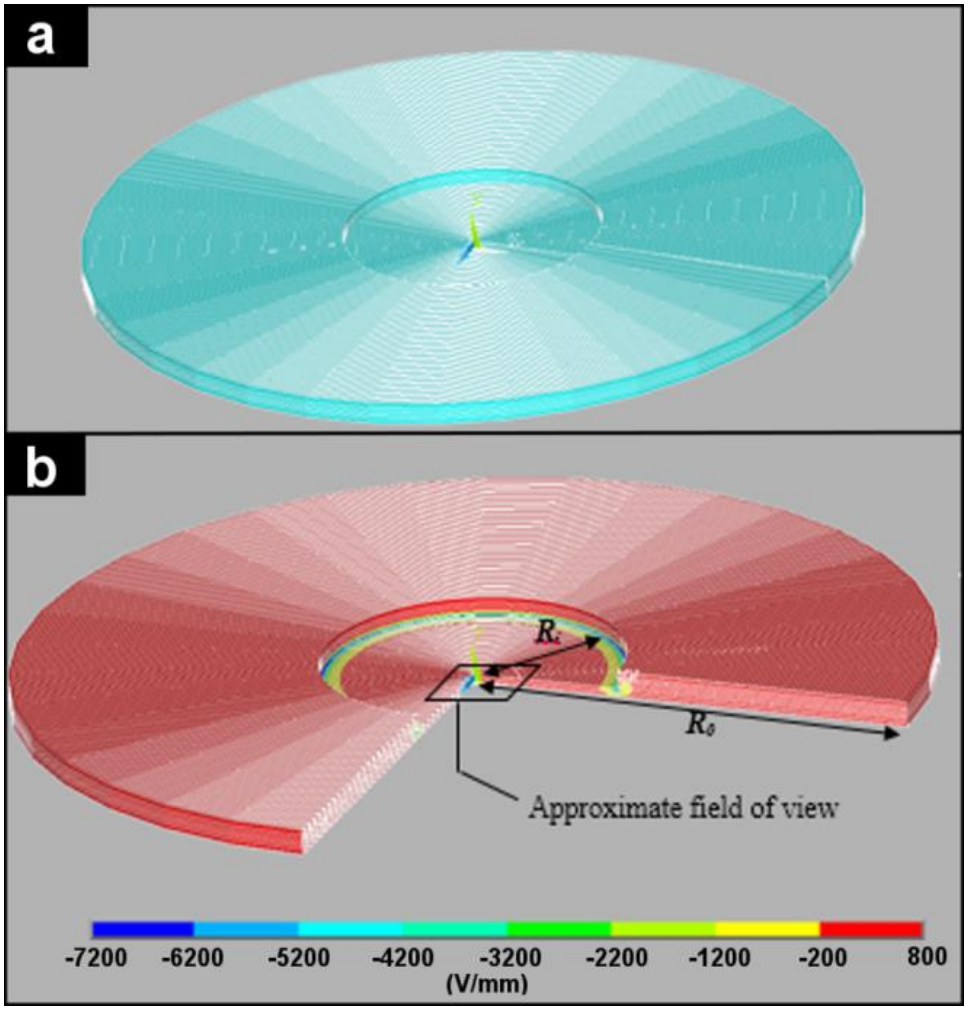

Figure 3.17. Finite element model mesh of the full pate bottom anode and the top lithium metal cathode with center hole removed (a), and the ANSYS simulated electrical field generated between them for a 3V applied potential differential (b).

3.4 Significance of Substrate Constraint Effect

Our experimental results show that substrate constraint have a strong effect on battery cycling performance. The high substantial strain within electrode will result capacity decrease. So we will make effort to minimize the substantial strain development. Surface treatment is an effective way to decrease the substantial strain development and can provide better adhesion between electrode film and substrate.

So in chapter IV, these findings on substrate constraint effect will be explored by a series of experiment including laser spallation test and delamination test.

CHAPTER IV

EFFECTS OF ELECTRODE ADHESION ON BATTERY PERFORMANCE

The adhesion quality between the electrode and substrate in lithium batteries has a significant effect on battery performance. Good substrate adhesion provides sufficient conductivity and bonding strength to withstand the strains associated with electrochemical cycling. On the other hand, poor adhesion can lead to bad conductivity and accelerated electrode material degradation in the form of microcracking or delamination that can cause dramatic capacity losses. Included in this chapter are the results of adhesion strength measurements on various electrode-substrates combinations performed using laser spallation and delamination tests, as well as results of battery performance testing using these same specimen variations. Testing results are followed by a discussion of the significance of the role of electrode adhesion and implications for future battery design optimization.

4.1 Specimen Preparation

For electrochemical and adhesion testing, three different electrode materials were investigated: amorphous silicon, traditional graphite, and a carbon nanotube-based composite. These specimens were prepared on three different copper substrates: untreated substrate, mechanically roughened substrates, and mildly chemically etched substrates.

4.1.1 Working Electrode Materials

Amorphous Si thin films were deposited by RF magnetron sputtering (Technics 4604 Sputter Coating System) onto a 400μm thick flat copper disk. A four inch diameter round target of pure Si (99.99%, Kurt J. Lesker) was used for the sputtering deposition. A 5 minute pre-sputtering procedure was used to remove any native silicon dioxide on the target before the final sputtering. Si thin films were deposited using a 300W RF power supply for a duration between 30 minutes and 60 minutes, depending on the desired thickness. During deposition, the chamber pressure was set at 25 mTorr with an Argon flow used as the processing gas. Film thicknesses for graphite electrode specimens were measured by profilometry (Veeco Dektak 8M Profilometer) to be in the range of 500 nm to 1000 nm. The initial silicon thin film weight was measured for each individual film and was typically around 1.0 mg.

Graphite electrodes were prepared by mixing 80 wt% graphite powder, 10 wt% carbon black, and 10 wt% polyvinylidene fluoride (PVDF) binders in a N-Methyl-2-pyrrolidone (NMP) solvent. The well-mixed slurry was deposited over the copper substrate, and a film casting doctor blade apparatus was used to skim the wet electrode material to a film thickness of 10 microns. The electrodes and substrates were then immediately put into a laboratory oven at 115ºC for 15 minutes.

Specimens containing the conductive CNTs as a graphite replacement were prepared in a similar manner. The CNTs used in this study were purchased in bulk commercially (Cheaptubes.com) and had diameters in a range of 60-80 nm and lengths in the range of 10-15 μm. The 80 wt% CNTs were first combined with 10 wt% carbon black and blended

in an industrial mixer a period of 12 hours. Next, 10 wt% PVDF binder and NMP solvents were injected into the mixture, which was then blended for an additional 12 hours. The slurry was then cast onto the copper substrates, skimmed to the proper thickness, and finally oven cured at 115ºC for 15 minutes.

4.1.2 Substrate Preparation

To investigate and quantify the effects of adhesion on battery performance, three type of surface treatments were applied to stock 400 μm thick copper sheets from which substrates were fabricated. Surface treatments included "untreated" (i.e. surface is "as fabricated"), mild chemical etching, and mechanically roughening. The untreated copper substrate has a smooth manufactured surface due to the rolling process. The chemically treated copper substrate was prepared under the following procedure: an etchant solution containing one part hydrogen peroxide was mixed with one part of hydrochloric acid (31% HCL) in a container. [76] The cleaned, (degreased) untreated substrates were placed into the etchant solution for a period of three minutes, and then were removed. Finally, the etched substrates were thoroughly rinsed with DI water and dried with an air gun. Mechanically roughened substrates were prepared by hand using 100 grit sand paper to abrade the copper surface. A consistent procedure was used to roughen each substrate, scrubbing the surface in every direction to make the roughness uniform across the specimen.

After treating the substrates, the surface of each was inspected under optical microscope to check for consistency in appearance. The resulting specimen surfaces are shown in Figure 4.1. The surface roughness of each was then also characterized under a profilometer (Veeco Dektak 8M), the results of which are shown in Figure 4.2.

Figure 4.1. Copper surface images under different treatment (left: untreated, middle: chemical treated, and right: mechanical treated)

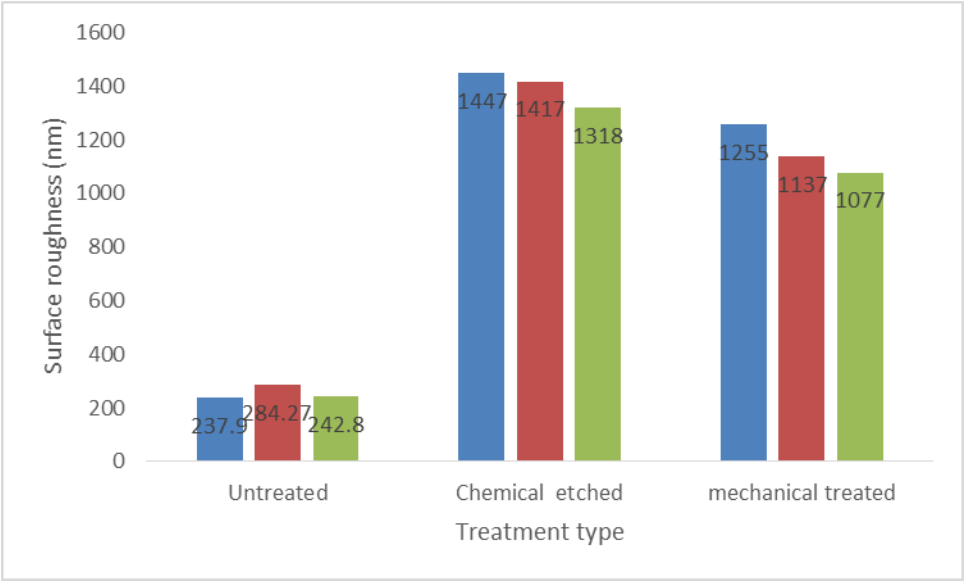

Figure 4.2 Surface roughness plot under different treatment

4.1.3 Custom Coin Cell Assembly

CR2032 coin cell was assembled in an Argon filled glove box. All parts, including cell cap, gasket, spring (Hohsen), and glass fiber separator (Advantec) were put into a 80°C

heated chamber (Buchi glass oven B585) and connected to a vacuum pump for eight hours to completely remove water moisture and evaporated solvent prior to assembly. For all coin cell configurations, a pure lithium metal disk (Sigma Aldrich) was used as the counter electrode.

An electrolyte consisting of 1M LiPF6-EC:DMC (1:2 by volume) was used throughout this work, with ca. 0.5 mL volume used for each cell. After stacking the layers and adding the electrolyte, a hand-operated crimping tool (Hohsen) was used to close and seal the coin cell batteries.

4.1.4 Laser Spallation Adhesion Specimen Preparation

There are basically four layers contained within specimens used for laser spallation test: the test film, the substrate, an absorbing layer and a confining layer. The schematic drawing is shown in Figure 4.3.

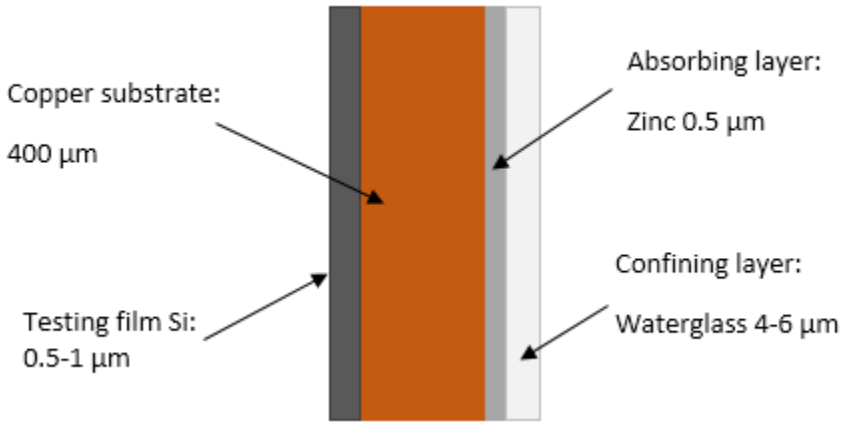

Figure 4.3. Schematic drawing of the thin film cross-section of specimens tested in the laser spallation set-up

The copper substrate is cut into 1.5 by 1.5 inch square samples. Amorphous Si thin films were deposited by RF magnetron sputtering onto a 400µm thick flat copper disk as indicated above. A thin zinc coating was deposited on the backside of copper substrate as the absorbing layer, and waterglass (Sigma Aldrich) was deposited on top of the absorbing layer using a spin coater just before the laser spallation test. As suggested by Gupta [45], waterglass thickness is optimized at 5 microns. To ensure the optimal absorbing layer thickness is used, waterglass thickness characterization was performed at different spinning speeds. These thickness characterization results are shown in Figure 4.4. And the triangle marker indicates the average thickness of the waterglass.

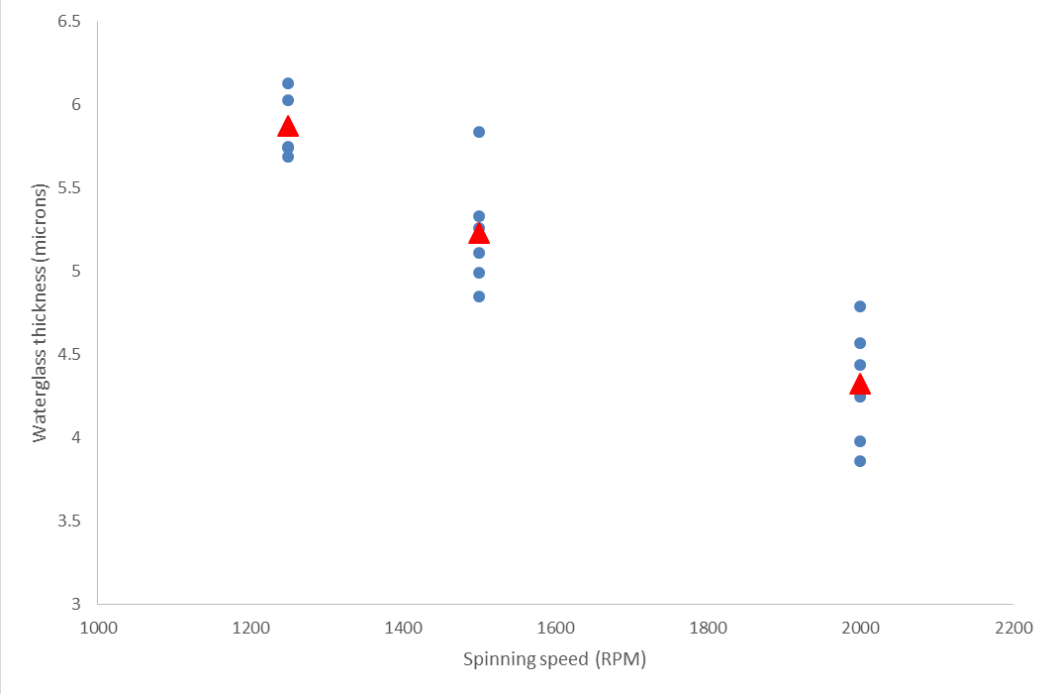

Figure 4.4. Waterglass thickness characterization under different spinning speeds

Graphite and CNT based electrode thin film are also tested in the laser spallation set-up, but we were unable to induce failure. The likely reason that we did not observe failure is

the limited power of our laser spallation system. To make the accurate measurement on these battery electrodes, we may replace with the more powerful laser or replace the copper substrate with more rigid one like fused quartz substrate.

4.1.5 Double Cantilever Beam Delamination Specimen Preparation

For the graphite electrode specimens, the laser spallation tests were unable to induce interfacial failure. Therefore, the adhesion measurements for this electrode-substrate was performed using a double cantilever beam delamination test. To prepare these specimens, first the copper substrate was cut into 1 inch by 3 inch rectangle specimens, and surface treatments were performed as described in the previous sections.

Graphite electrodes were prepared by mixing 80 wt% graphite powder, 10 wt% carbon black, and 10 wt% polyvinylidene fluoride (PVDF) binders in N-Methyl-2-pyrrolidone (NMP) solvent. The well-mixed slurry was deposited over the 1 inch by 3 inch copper substrate, and a film casting doctor blade apparatus was used to skim the wet slurry to a thickness of 10 microns. Then, two pieces of the coated substrates were placed with the electrode sides facing each other and were clamped together to form a "sandwich" type of specimen. The specimens were then immediately put into a laboratory oven at 115ºC for 20 minutes. Then we attached the 1 inch by 1 inch hinge on both sides of the specimen using JB Weld epoxy to serve as a specimen grip in the materials testing apparatus. A schematic of the samples are shown in Figure 4.5, and the actual specimen on MTS machine is shown in Figure 4.6.

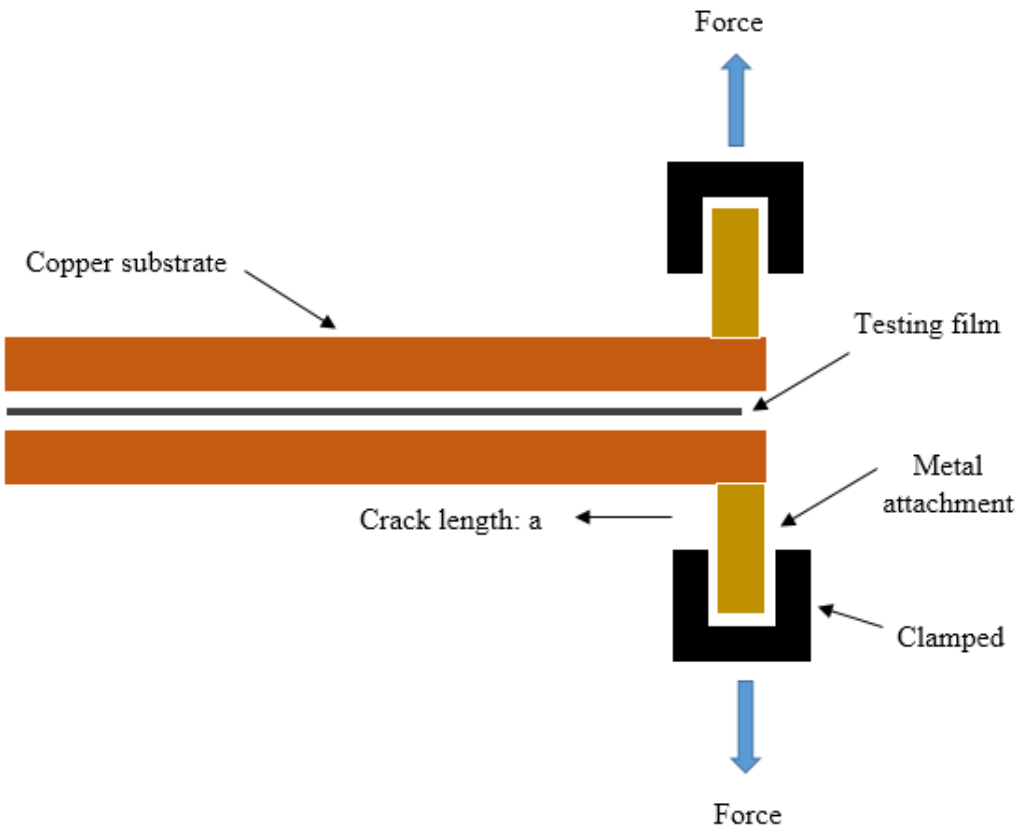

Figure 4.5. Schematic drawing of delamination test of graphite film specimen "sandwiched" by copper substrates

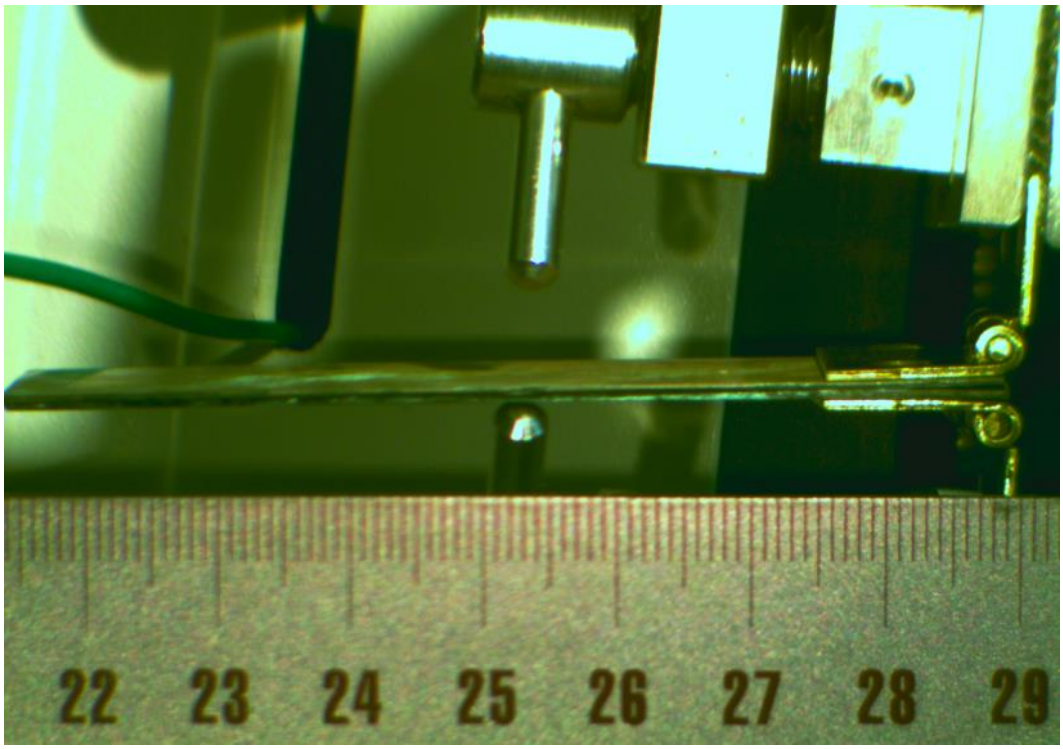

Figure 4.6. Actual specimen of graphite film "sandwiched" by copper substrates

4.2 Laser Spallation Testing of Electrodes

There are several methods to test the adhesion between film and substrate, and laser spallation technique laser spallation tests can provide a repeatable and quantified measurement of the film adhesion using a technique that is non-contact based. For extremely thin films, the method is preferred to peel tests (which require an adhesive layer often thicker than the film tested) or scratch tests (which provide less repeatability and can give results that are difficult to interpret). As a result, the adhesion strength results using this method are often much more accurate than for other methods. Laser spallation experimental testing was developed by Yuan and Gupta [71-73] to determine the tensile strength of thin film-substrate interfaces. Wang et al. [74] performed a parametric study on thin film adhesion strength which helped guide the specimen dimensions selected for

this work. The experiment setup has been discussed in chapter II. Based on Gupta and Wang's theory, at the interferometer alignment of maximum sensitivity, the light intensity on the detector is related to the fringe count, where I_{max} and I_{min} are the maximum and minimum intensities of the interference fringes and φ is the phase angle.

$$I(t) = \frac{I_{max}+I_{min}}{2} + \frac{I_{max}-I_{min}}{2}\sin(2\pi n(t)+\varphi) \quad (1)$$

The surface displacement is obtained in terms of the fringe count.

$$u(t) = \frac{\lambda_0 n(t)}{2} \quad (2)$$

The fringe count is determined from the output of the photodiode detector. (Eq. 1) One complete fringe shift corresponds a displacement of $\frac{\lambda_0}{2}$. Once the free surface displacement is obtained from the interferometric measurements, the compressive stress propagating from absorbing layer towards the substrate can be calculated using simple 1-D wave mechanics, where ρ is the density and c is the longitudinal wave speed of the substrate.

$$\sigma = -\frac{1}{2}(\rho c)\frac{\partial u}{\partial t} \quad (3)$$

4.2.1 Substrate Stress Characterization

Prior to any measurement, a careful laser alignment routine was performed to make sure that Michaelson interferometer can pick-up the proper signal. Then, a series of experiments were performed to characterize the laser power and substrate stress response. A typical

substrate displacement and stress characterization is shown in Figure 4.7 and Figure 4.8, respectively.

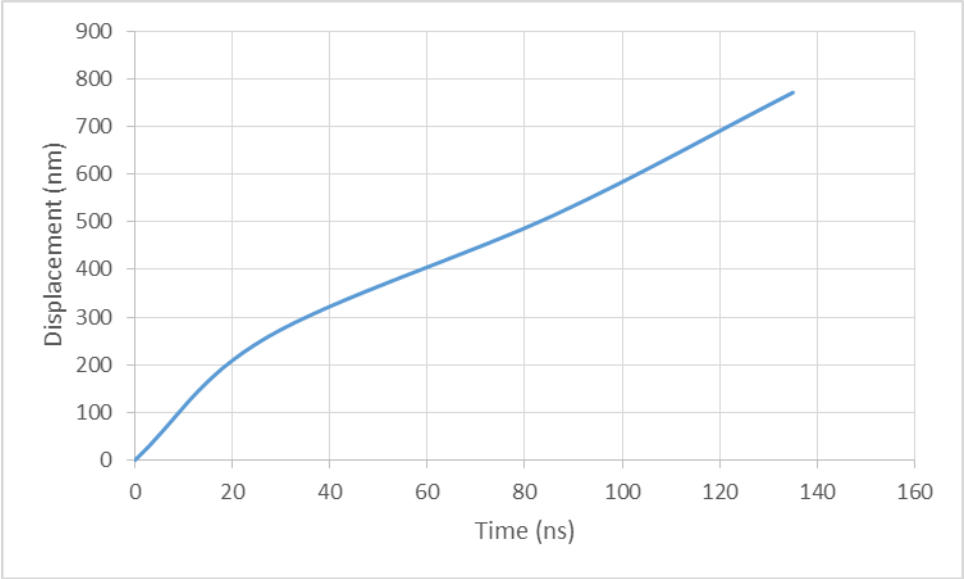

Figure 4.7. A typical displacement profile for a 400µm copper substrate

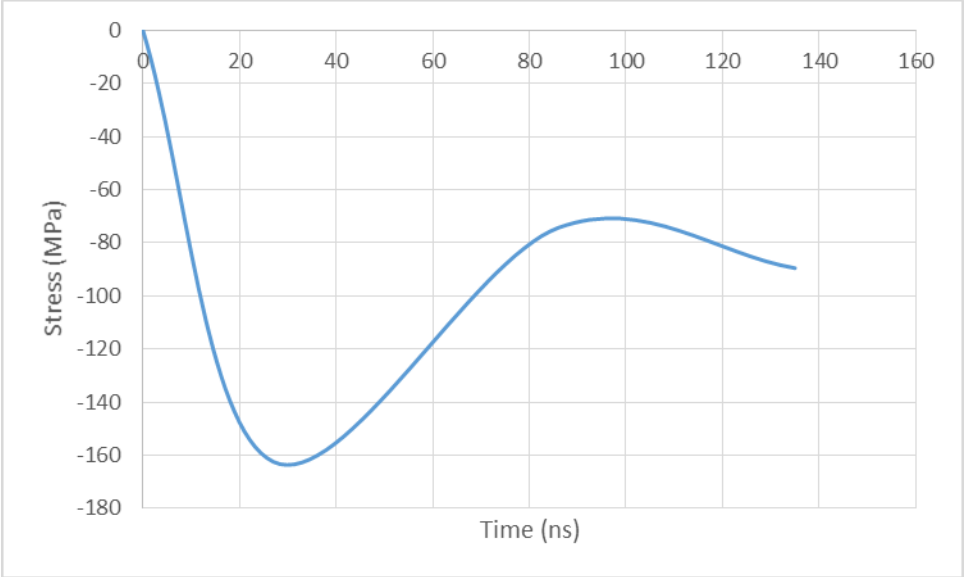

Figure 4.8. A typical stress profile for a 400µm copper substrate

And the maximum substrate stress values for different laser power levels are calculated in Figure 4.9

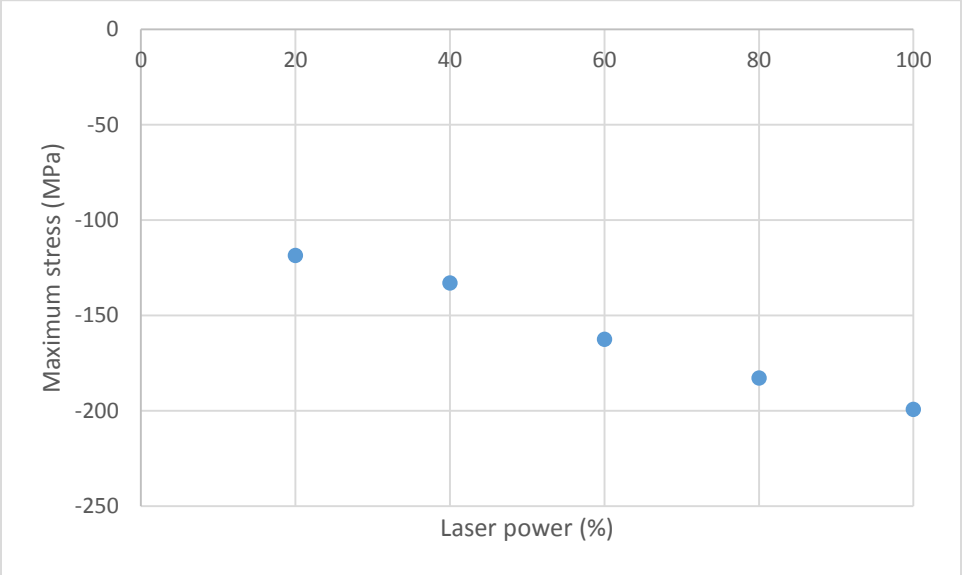

Figure 4.9. Maximum substrate stress values versus different laser power levels of 400 microns copper substrate

4.2.2 Adhesion Strength Results for Si Electrode Films

Once the substrate stress is characterized, 500nm thick silicon thin film on 400μm copper substrate are carried out the test. There are still three different surface treatment variations. The specimens are under different power level of the YAG laser. And typical images after spallation is shown in Figure 4.10 to Figure 4.12.

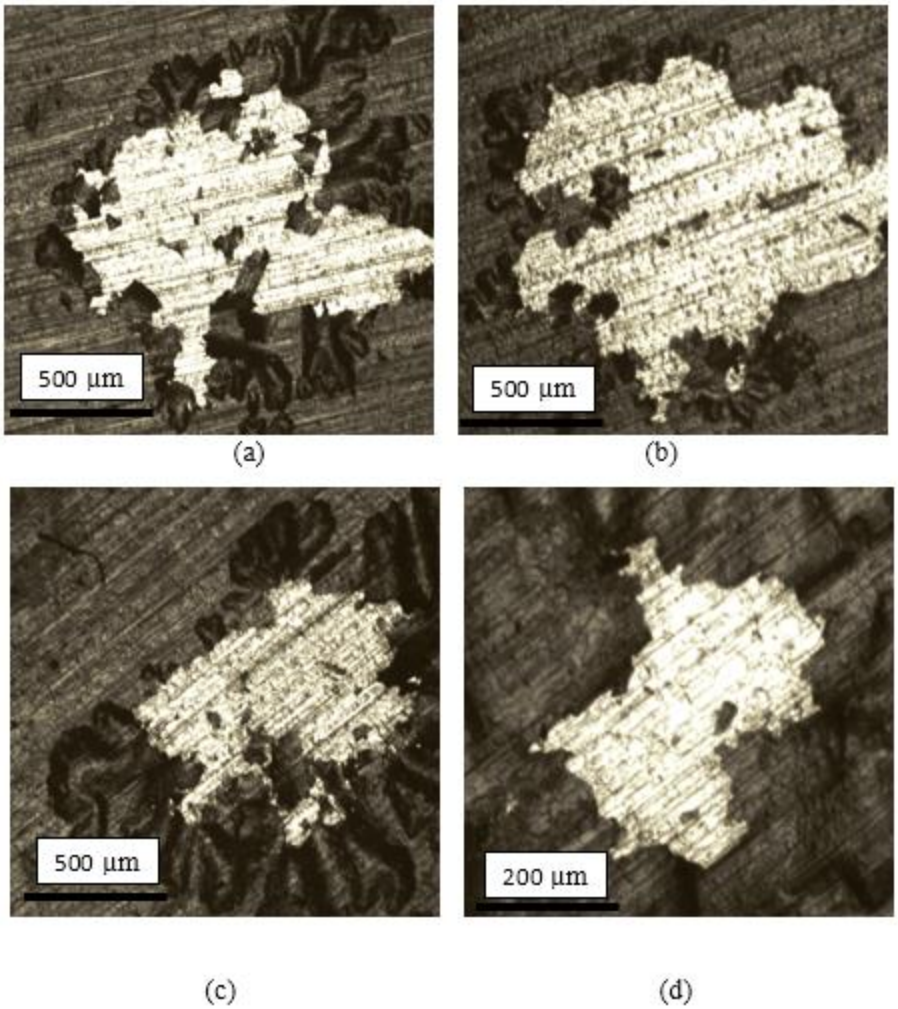

Figure 4.10. Typical image of 500 nm silicon thin film on 400µm thick untreated copper substrate: (a) 80% laser power, (b) 60% laser power, (c) 40% laser power, and (d) 30% laser power laser power. The diameter of the laser spot is about 1-1.2mm.

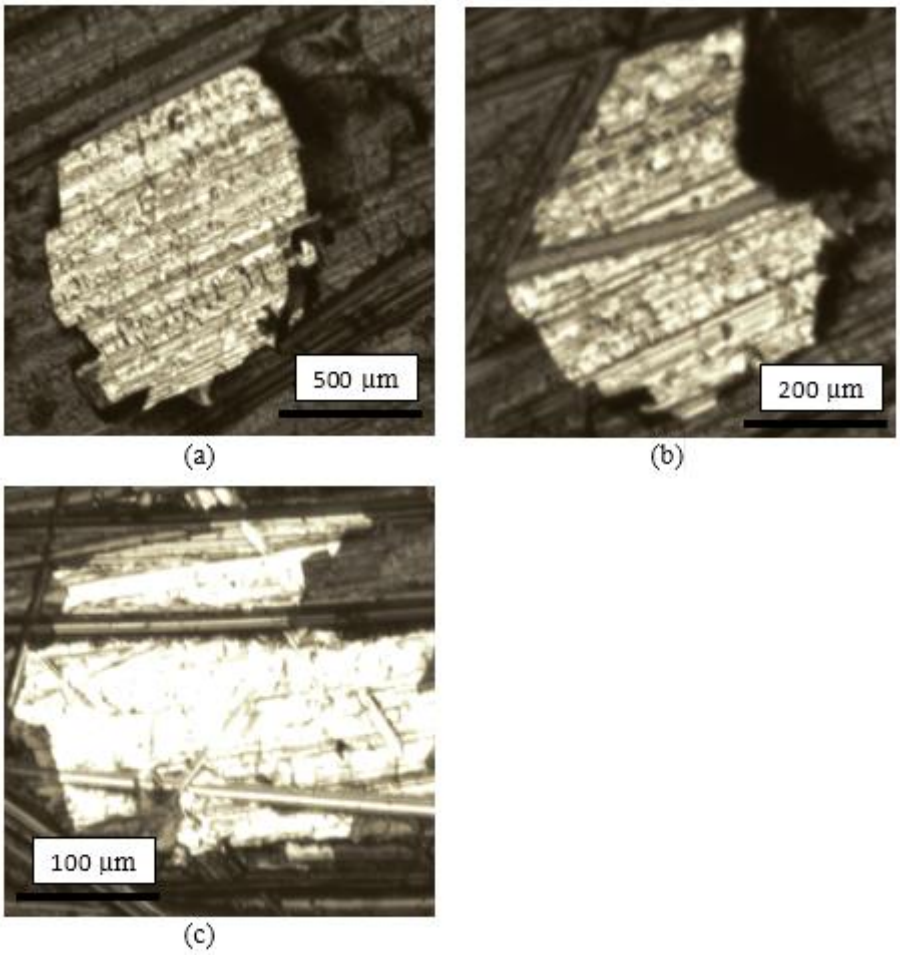

Figure 4.11. Typical image of 500 nm silicon thin film on 400µm thick mechanical treated copper substrate with randomly scrubbed method: (a) 60% laser power, (b) 50% laser power, and (c) 40% laser power. The diameter of the laser spot is about 1-1.2mm.

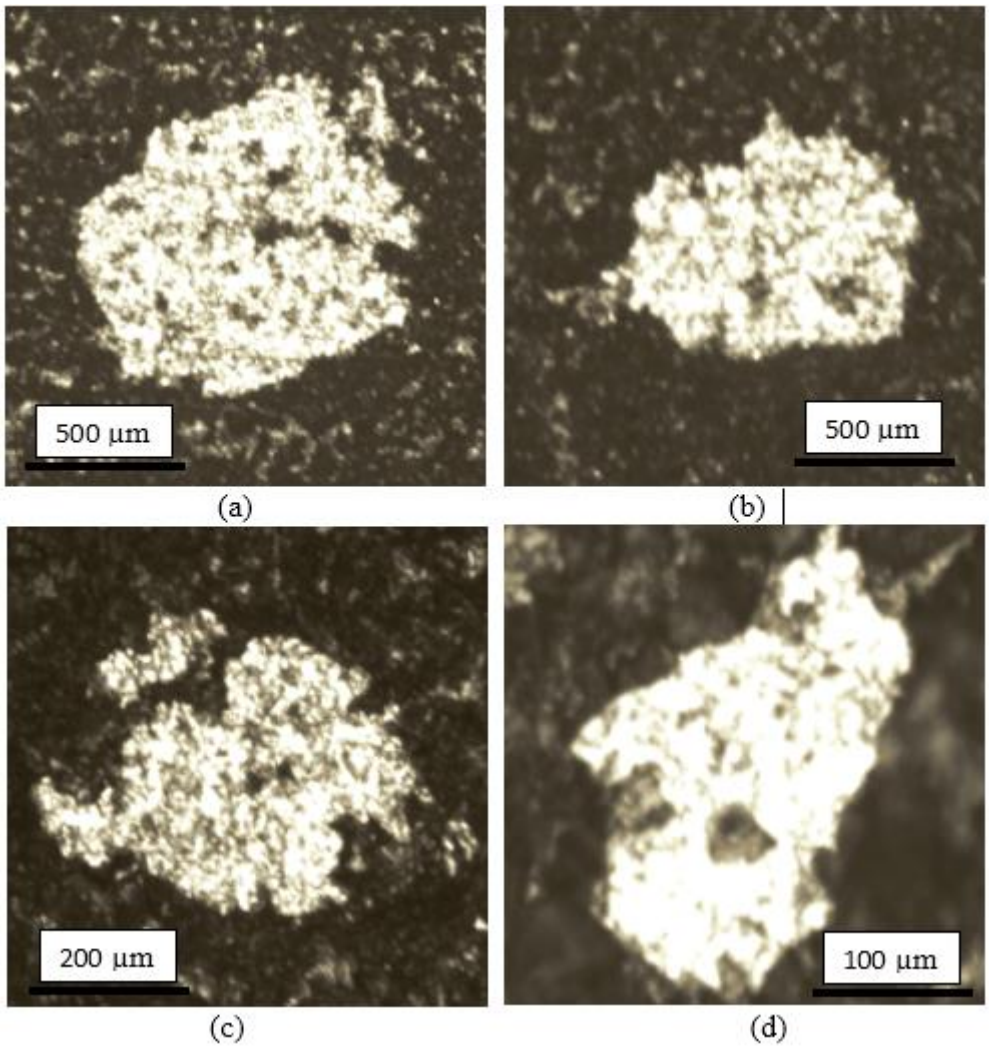

Figure 4.12. Typical image of 500 nm silicon thin film on 400µm thick chemical treated copper substrate: (a) 80% laser power, (b) 60% laser power, (c) 50% laser power and (d) 45% laser power. The diameter of the laser spot is about 1-1.2mm.

So, based on the inspection of spallation images shown above, the minimum power to induce the spallation for the untreated, mechanical treated and chemical treated copper substrate is roughly 30%, 40% and 45% respectively. Below these thresholds, no interfacial film damage was observed.

Based on the assumption of a 1-dimensional wave propagation through the substrate thickness, a simplified equivalent of Newton's second law can be used to calculate the interface, which is equal to the mass density of the film multiplied by the acceleration. The equation is given by:

$$\sigma_{interface} = -(ph)_{film} \frac{\partial^2 u}{\partial t^2} \qquad (4)$$

And the typical interface stress of three different substrate treatment is calculated below:

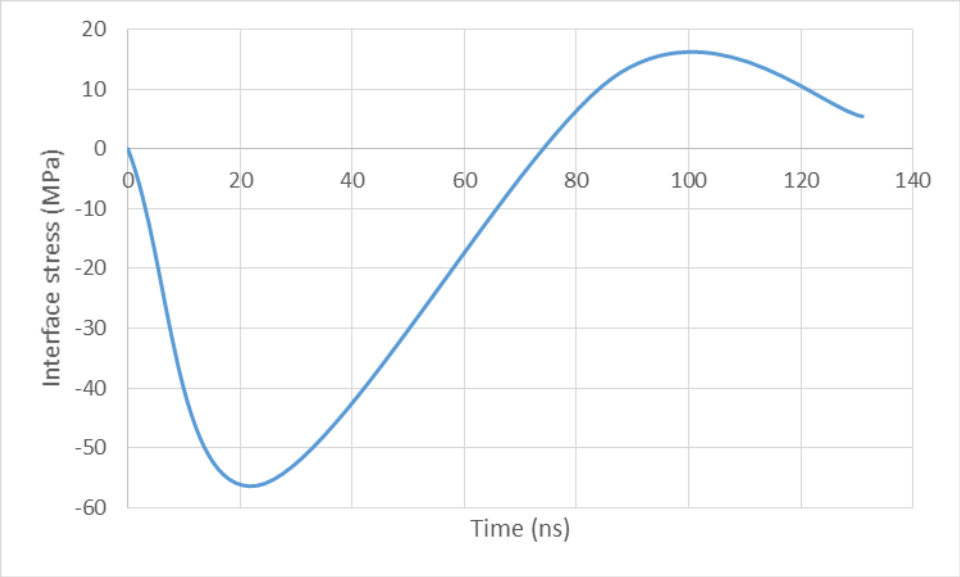

Figure 4.13. A typical interface stress profile of untreated copper substrate

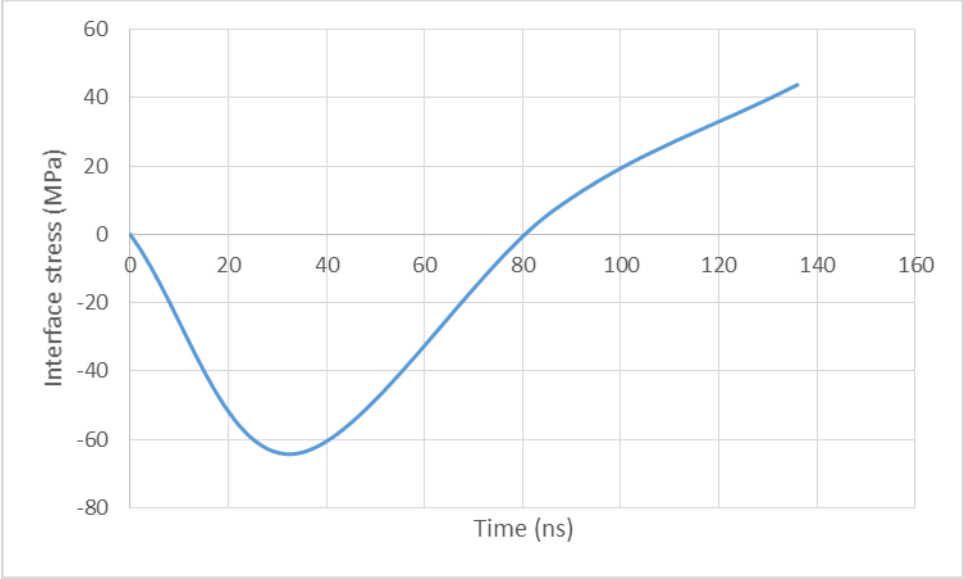

Figure 4.14. A typical interface stress profile of mechanical treated copper substrate

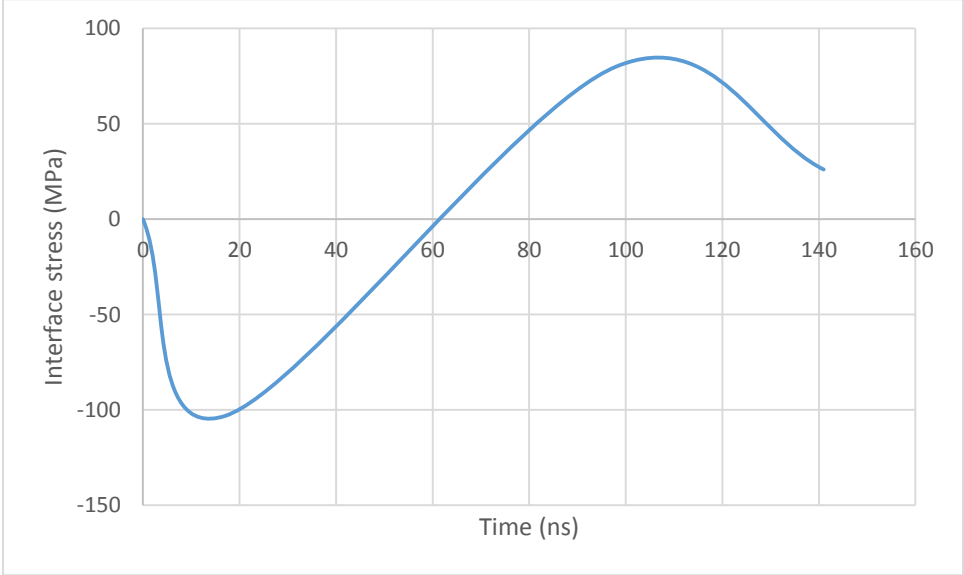

Figure 4.15. A typical interface stress profile of chemical treated copper substrate

4.3 Delamination Testing of Electrodes

After specimens were prepared, a Shimadzu universal materials testing machine (EZ Test model) was used to perform the delamination test, experiment setup is shown in Figure 4.16. The loading rate is set to 0.5mm/min. *In-situ* images are taken once every second to record the crack length on the specimen.

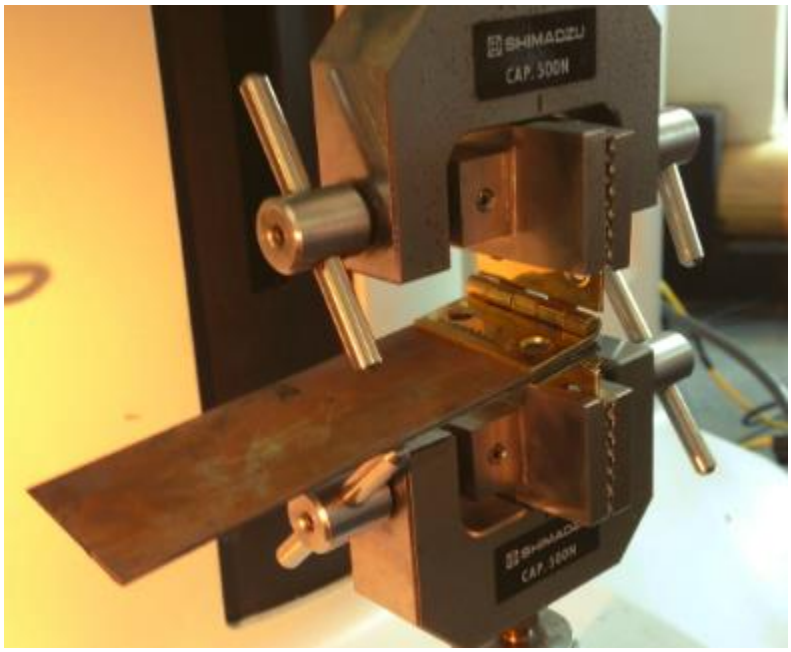

Figure 4.16. Actual experimental set-up for delamination test

The measured displacement vs. load plot for untreated, mechanically treated and chemical treated substrate is shown in Figure 4.17-4.19.

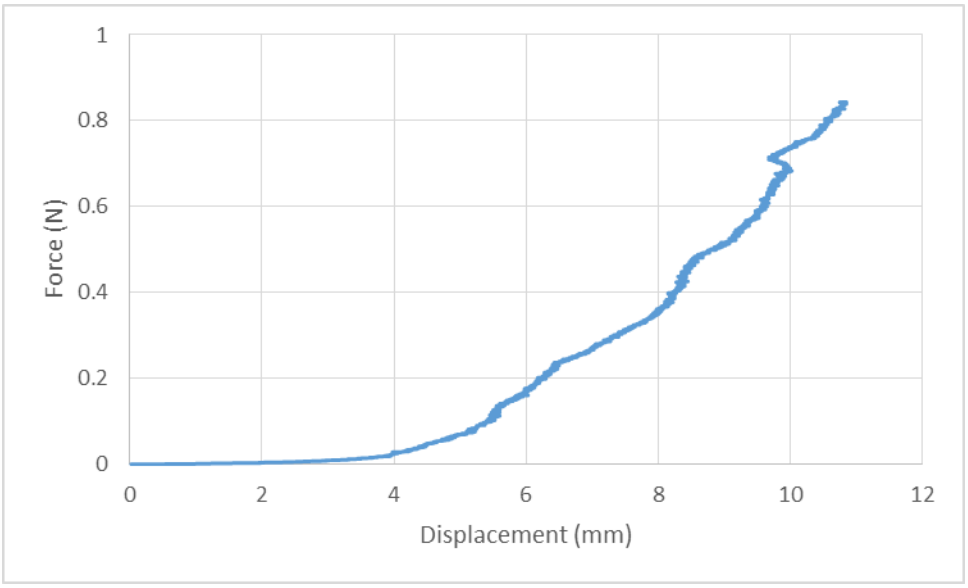

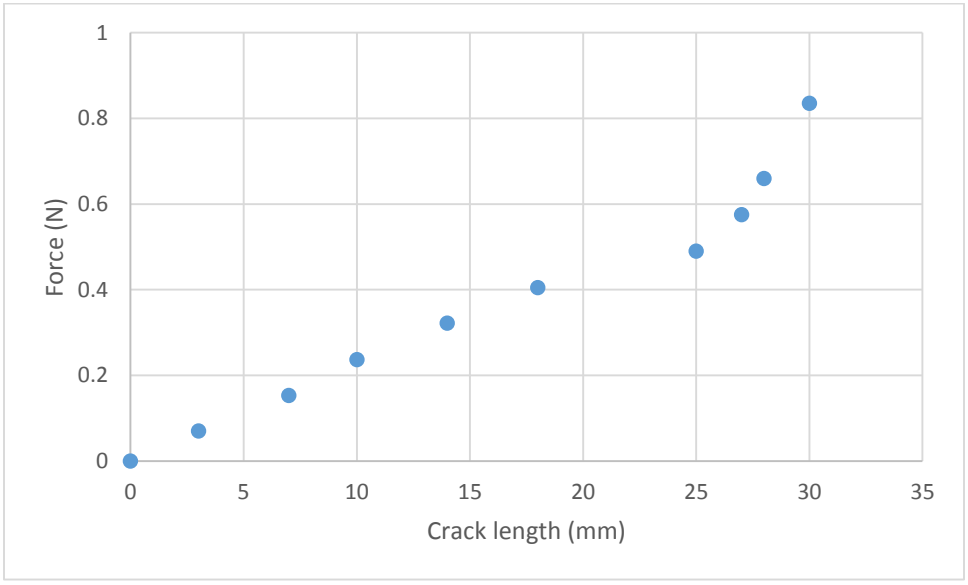

Figure 4.17. Measured load versus displacement (up) and crack length (bottom) plot of untreated copper substrate

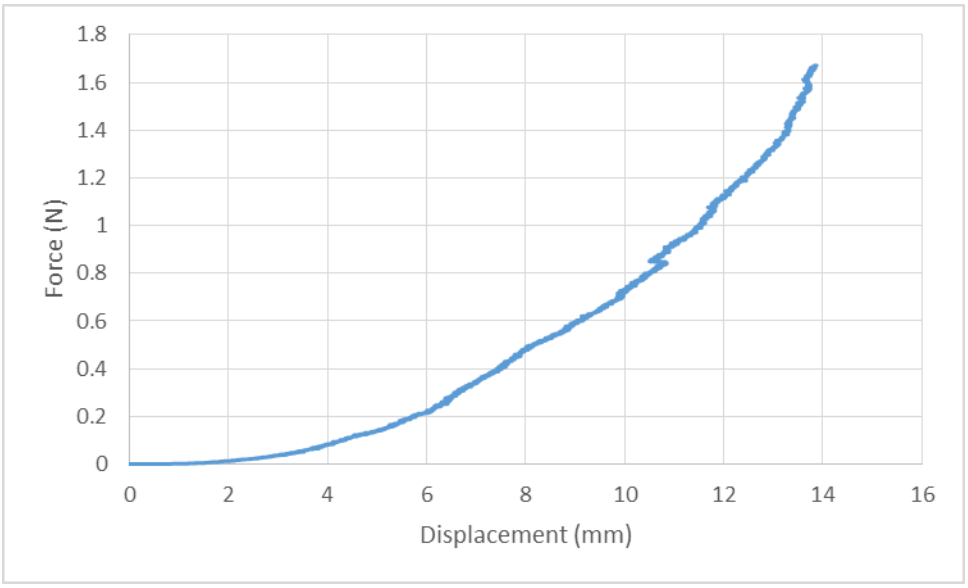

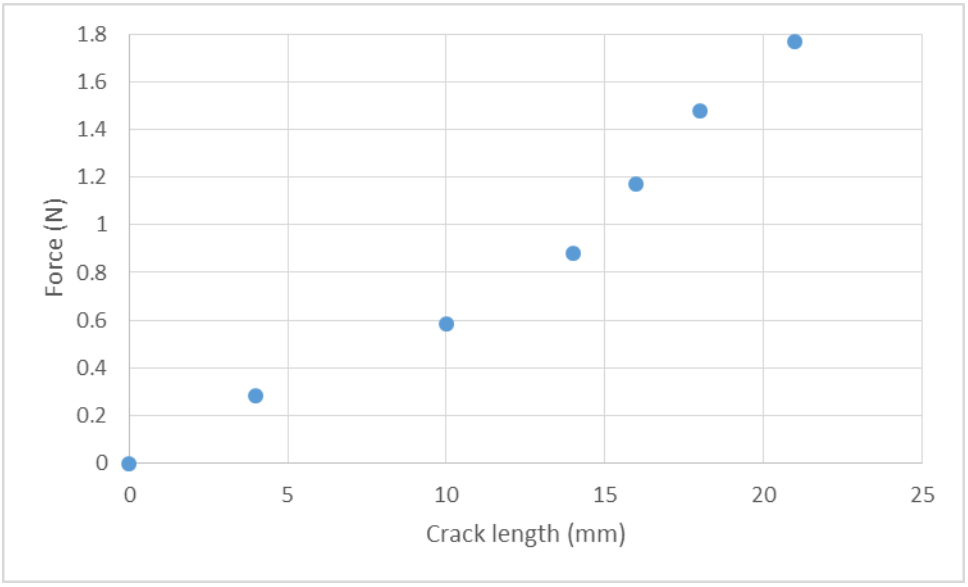

Figure 4.18. Measured load versus displacement (up) and crack length (bottom) plot of mechanically treated copper substrate

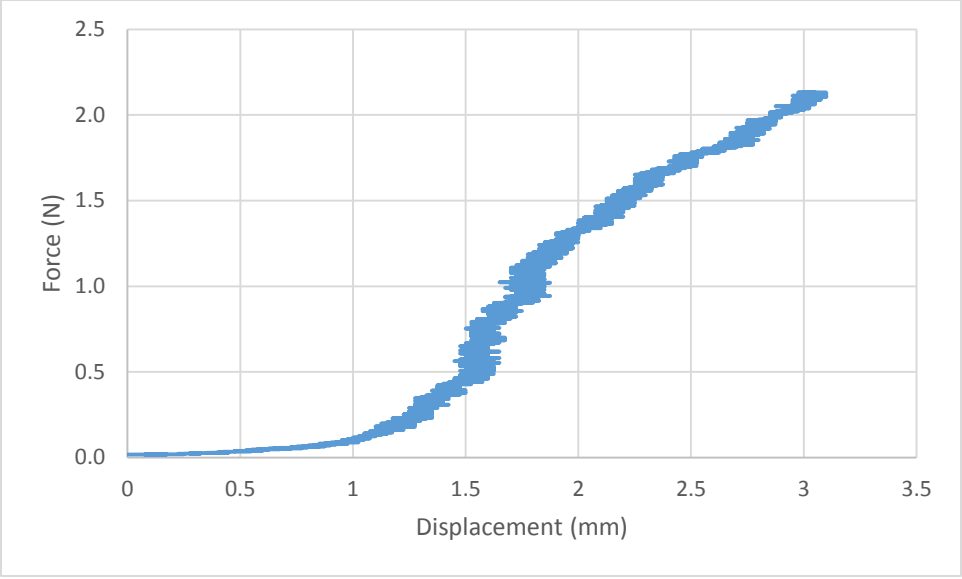

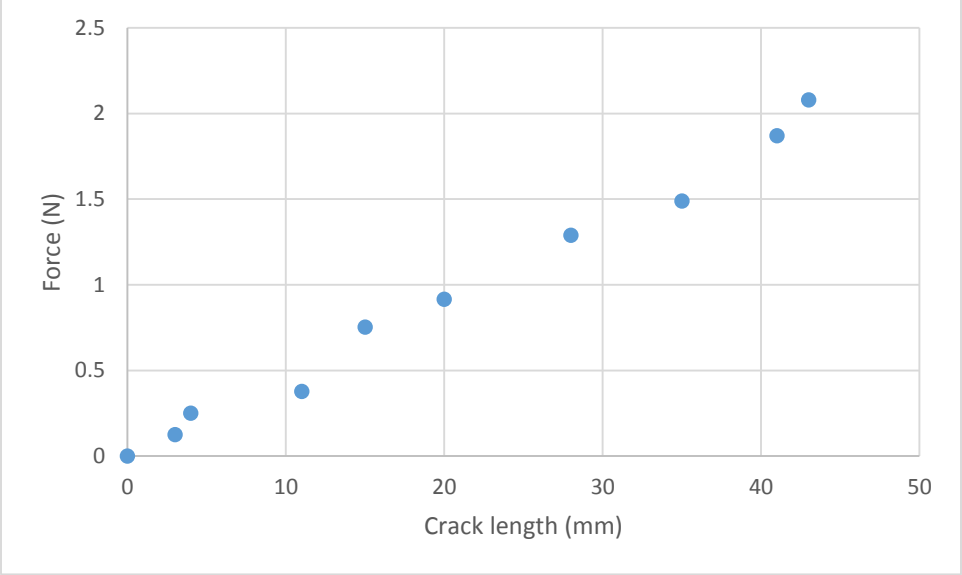

Figure 4.19. Measured load versus displacement (up) and crack length (bottom) plot of chemical treated copper substrate

4.4 Substrate Adhesion Effects on Battery Performance

In chapter III, we discussed the *in-situ* strain development on battery electrode, and we found that battery capacity decrease dramatically with the increase of the electrode strain during the charging/discharging cycles. The decrease in performance associated with these electrode deformations is likely a symptom of material degradation (microcracking). Such material breakdowns could be potentially somewhat mitigated through improvement of electrode-substrate adhesion. To test this hypothesis, we investigate the substrate adhesion effects on battery performance in this section. As indicated in previous sections, substrates for the electrode were treated in three different ways, untreated, mechanically roughened, and chemically etched, to induce different adhesion characteristics.

Silicon, graphite and CNT based electrodes were prepared in the same manner as with the previous tests. Electrochemical testing conditions were used identical to that presented in Chapter III. The results of this testing gives the discharge capacity versus cycle numbers plots for the different substrate treatment and electrode material variations (multiple samples tested for each). Figures 4.20-4.22 shows the normalized discharge capacity vs. cycle numbers for silicon, graphite, and the CNT-based electrodes.

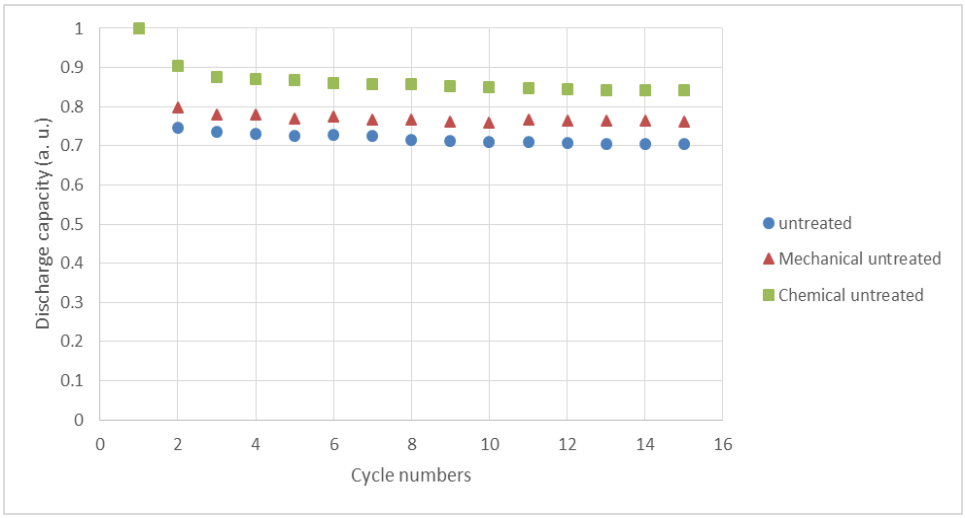

Figure 4.20. Normalized discharge capacity for silicon thin film working electrode as the number of electrical charge/discharge cycles increases: untreated copper substrate, mechanical treated copper substrate and chemical treated copper substrate

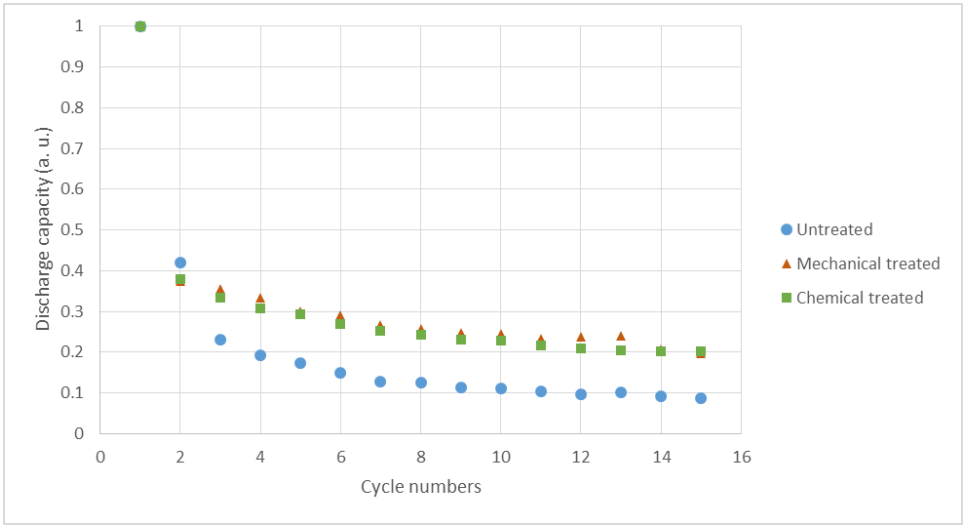

Figure 4.21. Normalized discharge capacity for graphite working electrode as the number of electrical charge/discharge cycles increases: untreated copper substrate, mechanical treated copper substrate and chemical treated copper substrate.

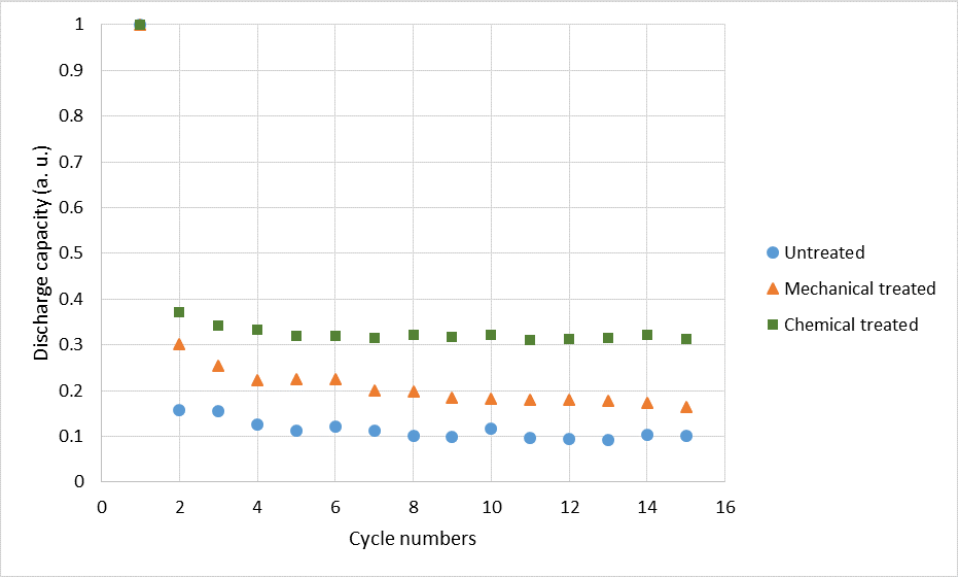

Figure 4.22. Normalized discharge capacity for carbon nanotube based working electrode as the number of electrical charge/discharge cycles increases: untreated copper substrate, mechanical treated copper substrate and chemical treated copper substrate

The trend is very clear for all three electrodes; the capacity loss rate on the untreated substrate was the highest among the three variations, while the capacity loss rate on chemically etched substrate was the lowest among of them.

Silicon thin film electrodes surface optical images are taken after 15 electrical cycles on untreated, mechanically treated and chemical treated substrates. Figure 4.23 shows that on untreated substrate, one wide through-thickness cracks form on the silicon thin film, while we can also see the cracks on mechanically treated and chemical treated substrate, but apparently, those cracks are not as deep or wide as the untreated ones. Those cracks are likely driven by the inadequate adhesion between silicon film and copper substrate. And we can see the adhesion improvement from both mechanically treated and chemical treated substrates which coincide with our laser spallation and delamination test results.

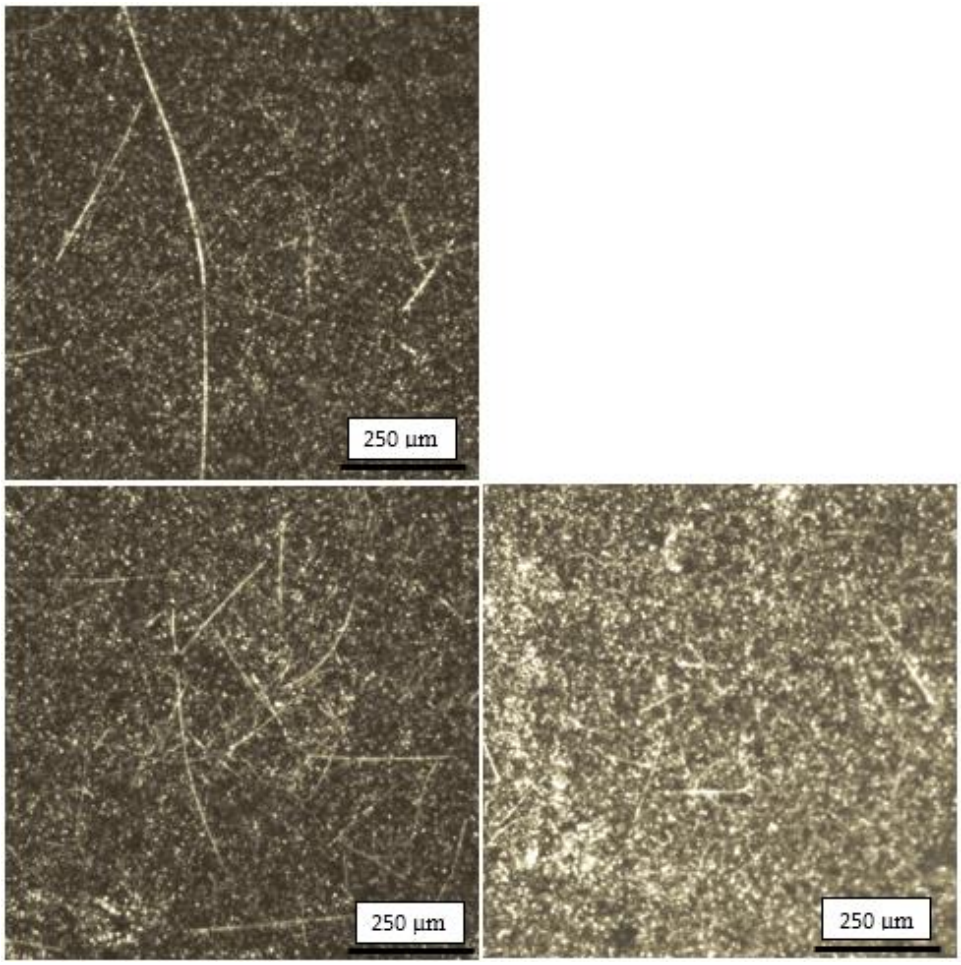

Figure 4.23. Silicon surface images after 15 electrical cycles on untreated substrate (up left), mechanically treated substrate (bottom left) and chemical treated substrate (bottom right)

4.5 Significance of Electrode Adhesion Effects

The results completely match the findings in the previous laser spallation and delamination results. So, we can draw the following conclusions: 1) substrate treatment can improve the adhesion between film and substrate; 2) chemical etched substrates demonstrated slightly

better adhesion than the mechanically roughened substrate, and much better than that with no surface treatment; 3) surface treatment on electrode substrate can decrease the capacity loss while improving the battery performance.

Since the surface treatment can really improve the adhesion between electrode film and substrate, and the adhesion can impact the battery performance dramatically. So this will give battery designer a great suggestion. Surface treatment is an effective way to improve adhesion with minimum cost. Also, finding alternative binders are another approach to achieve a better adhesion.

CHAPTER V

CONCLUSIONS AND FUTURE DIRECTIONS

5.1 Conclusion

This dissertation investigated the effects of substrate constraint on substantial strain development within lithium battery electrode. A digital image correlation analysis were performed on a series number of images taken on electrode surface. With amorphous silicon as working electrode, the most significant changes in the in-plane strain observed for the anode corresponded with images correlated between the fully charged and fully discharged states. Cracking of the thin amorphous silicon layer is likely driven by inadequate adhesion with the substrate. For certain silicon layer thicknesses and sputter coating deposition conditions (higher temperatures and rates), it was also observed that the residual film stresses that developed were sufficient to cause delamination.

For both graphite and CNT-based electrodes, the strains within electrodes deposited on copper foil substrates were significantly larger than strains measured for the copper disk substrate specimens; an expected effect due to the greater rigidity of the disk. We also found that as the number of charge/discharge cycles increases, there is a continual increase in the residual strains within the electrodes. In other words, to achieve the same potential charge at the end of each cycle, larger electrode deformations are required as the cycle

number grows. At the same time, battery capacity decreases as the number of cycles increase. And the results are verified by finite element analysis.

Throughout the results of adhesion strength measurements on various electrode-substrates combinations performed on laser spallation and delamination test, and the comparable battery cycling test with the same specimen variations, we can conclude that substrate treatment can improve the adhesion between film and substrate, chemical etched substrates demonstrated slightly better adhesion than the mechanically roughened substrate, and much better than that with no surface treatment; surface treatment on electrode substrate can decrease the capacity loss while improving the battery performance.

5.2 Future Directions

We studied adhesion quality between film and substrate, and mechanical roughened and chemical etched surface treatment are investigated. Future projects should include studies on more substrate treatment development method. For example, laser micro-texturing is a great alternative to create unique and more oriented surface profiles, and it should improve the adhesion effectively.

We also quantified the adhesion strength between silicon electrode film and copper substrate, and there are many other potential electrode-substrates combinations that can be studied and quantified. Battery designers and other researchers can design and fabricate more efficient and powerful batteries based on the accurate adhesion strength measurement.

REFERENCES

[1] M. Armand, J.-M. Tarascon Building better batteries, Nature 451, 652-657 (7 February 2008)

[2] Languang Lu, Xuebing Han, Jianqiu Li, Jianfeng Hua, Minggao Ouyang, A review on the key issues for lithium-ion battery management in electric vehicles, Journal of Power Sources, Volume 226, 15 March 2013, Pages 272-28

[3] P. Poizot, S. Laruelle, S. Grugeon, L. Dupont & J-M. Tarascon, Nano-sized transition-metal oxides as negative-electrode materials for lithium-ion batteries, Nature 407, 496-499 (28 September 2000)

[4] Yoshio Nishi, Lithium ion secondary batteries; past 10 years and the future, Journal of Power Sources, Volume 100, Issues 1–2, 30 November 2001, Pages 101-106

[5] Bruno Scrosati, Jürgen Garche, Lithium batteries: Status, prospects and future, Journal of Power Sources, Volume 195, Issue 9, 1 May 2010, Pages 2419-2430,

[6] Bruno Scrosati,Jusef Hassoun,and Yang-Kook Sun Lithium-ion batteries. A look into the future, Energy Environ. Sci., 2011,4, 3287-3295

[7] Charles de las Casas, Wenzhi Li, A review of application of carbon nanotubes for lithium ion battery anode material, Journal of Power Sources, Volume 208, 15 June 2012, Pages 74-85

[8] Wei-Jun Zhang, A review of the electrochemical performance of alloy anodes for lithium-ion batteries, Journal of Power Sources, Volume 196, Issue 1, 1 January 2011, Pages 13-24, ISSN 0378-7753

[9] Doron Aurbach, Review of selected electrode–solution interactions which determine the performance of Li and Li ion batteries, Journal of Power Sources, Volume 89, Issue 2, August 2000, Pages 206-218

[10] Bruno Scrosati, Recent advances in lithium ion battery materials, Electrochimica Acta, Volume 45, Issues 15–16, 3 May 2000, Pages 2461-2466

[11] Arumugam Manthiram, Materials Challenges and Opportunities of Lithium Ion Batteries The Journal of Physical Chemistry Letters 2011 2 (3), 176-184

[12] John B. Goodenough and Youngsik Kim, Challenges for Rechargeable Li Batteries Chemistry of Materials, 2010 22 (3), 587-603

[13] P.G. Balakrishnan, R. Ramesh, T. Prem Kumar, Safety mechanisms in lithium-ion batteries, Journal of Power Sources, Volume 155, Issue 2, 21 April 2006, Pages 401-414

[14] Thackeray, Thomas, and Whittingham (March 2000). Science and Applications of Mixed Conductors for Lithium Batteries. Materials Research Society.

[15] S. Flandrois, B. Simon. Carbon. Vol. 37, issue 2 1999

[16] M. Liang and L. Zhi, J. Mater. Chem. 2009, 19, 5871-5878

[17]T. Nagaura and K. Tozawa, Progress in Batteries and Solar Cells. Vol. 9, 1990.

[18].Yuqin, C.H., Li; Lie, Wu; Tianhong, Lu Irreversible capacity loss of graphite electrode in lithium-ion batteries. Journal of Power Sources, 1997. 68: p. 187-190.

[19]. Joho, F., et al., Key factors for the cycling stability of graphite intercalation electrodes for lithium-ion batteries. Journal of Power Sources, 1999. 81-82: p. 243-247.
[20].Shim, J. and K.A. Striebel, Effect of electrode density on cycle performance and irreversible capacity loss for natural graphite anode in lithium-ion batteries. Journal of Power Sources, 2003. 119-121: p. 934-937.
[21].Winter, M., P. Novák, and A. Monnier, Graphites for Lithium-Ion Cells: The Correlation of the First-Cycle Charge Loss with the Brunauer-Emmett-Teller Surface Area. Journal of The Electrochemical Society, 1998. 145(2): p. 428-436.
[22]. Joho, F., et al., Relation between surface properties, pore structure and first-cycle charge loss of graphene as negative electrode in lithium-ion batteries. Journal of Power Sources, 2001. 97-98: p. 78-82.
[23]. Manev, V., et al., Effect of electrode porosity on the performance of natural Brazilian graphite electrodes. Journal of Power Sources, 1995. 57: p. 133-136.
[24]. Novák, P., et al., The complex electrochemistry of graphite electrodes in lithium-ion batteries. Journal of Power Sources, 2001. 97-98: p. 39-46.
[25] I. Yoshio, Tin-Based Amorphous Oxide: A High-Capacity Lithium-Ion-Storage Material Science 30 May 1997: 276 (5317), 1395-1397
[26] Masaki Yoshio et al, Carbon-Coated Si as a Lithium-Ion Battery Anode Material J. Electrochem. Soc. 2002 volume 149, issue 12, A1598-A1603
[27] X. P. Gao, , J. L. Bao, G. L. Pan, H. Y. Zhu, P. X. Huang, F. Wu, and, D. Y. Song The Journal of Physical Chemistry B 2004 108 (18), 5547-5551
[28] Li-Feng Cui, Yuan Yang, Ching-Mei Hsu, and Yi Cui, Carbon−Silicon Core−Shell Nanowires as High Capacity Electrode for Lithium Ion Batteries Nano Letters 2009 9 (9), 3370-3374
[29] D. Larcher, S. Beattie, M. Morcrette, K. Edstroem, J.C. Jumas, and J.M. Tarascon, Recent Findings and Prospects in the Field of Pure Metals as Negative Electrodes for Li-Ion Batteries. Journal of Materials Chemistry, 17(36): 3759-3772. (2007)
[30]Boukamp, B. A., Lesh, G. C. & Huggins, R. A. All-solid lithium electrodes with mixed-conductor matrix. J. Electrochem. Soc. 128, 725– 729 (1981).
[31] M.N. Obrovac and L. Christensen, Structural Changes in Silicon Anodes during Lthium Insertion/Extraction. Electrochemical and Solid State Letters, 7(5): A93-A96. (2004)
[32] C.M. Park, J.H. Kim, H. Kim, and H.J. Sohn, Li-Alloy Based Anode Materials for Secondary Batteries. Chemical Society Reviews, 39(8): 3115-3141. (2010)
[33] U. Kasavajjula, C.S. Wang, and A.J. Appleby, Nano- and Bulk-Silicon-Based Insertion Anodes for Lithium-Ion Secondary Cells. Journal of Power Sources, 163(2): 1003-1039. (2007)
[34]Hunjoon Jung, Min Park, Shin Hee Han, Hyuck Lim, Seung-Ki Joo, Amorphous silicon thin-film negative electrode prepared by low pressure chemical vapor deposition for lithium-ion batteries, Solid State Communications, Volume 125, Issues 7–8, February 2003
[35] J. Li, R.B. Lewis, and J.R. Dahn, Sodium carboxymethyl cellulose - A potential binder for Si negative electrodes for Li-ion batteries. Electrochemical and Solid State Letters, 10(2): A17-A20. (2007)

[36] L.J. Fu, H. Liu, C. Li, Y.P. Wu, E. Rahm, R. Holze, H.Q. Wu, Surface modifications of electrode materials for lithium ion batteries, Solid State Sciences, Volume 8, Issue 2, February 2006
[37] J.P. Maranchi, A.F. Hepp, and P.N. Kumta, High Capacity, Reversible Silicon Thin-Film Anodes for Lithium-Ion Batteries. Electrochemical and Solid State Letters, 6(9): A198-A201. (2003)
[38] C.K. Chan, H.L. Peng, G. Liu, K. McIlwrath, X.F. Zhang, R.A. Huggins, and Y. Cui, High-Performance Lithium Battery Anodes using Silicon Nanowires. Nature Nanotechnology, 3(1): 31-35. (2008)
[39] H. Kim, M. Seo, M.H. Park, and J. Cho, A Critical Size of Silicon Nano-Anodes for Lithium Rechargeable Batteries. Angewandte Chemie-International Edition, 49(12): 2146-2149. (2010)
[40] X. Xiao, P. Liu, M.W. Verbrugge, H. Haftbaradarab, and H. Gao, Improved Cycling Stability of Solicon Thin Film Electrodes through Patterning for High Energy Density Lithium Batteries. Journal of Power Sources, 196(3): 1409-1416. (2010)
[41] H. Wu, G. Chan, J.W. Choi, I. Ryu, Y. Yao, M.T. McDowell, S.W. Lee, A.Jackson, L. Hu, and Y. Cui, Six Thousand Electrochemical Cycles of Double-Walled Silicon Nanotube Anodes for Lithium Ion Batteries. 7,310-315 Nano Letters (2012)
[42] Mao, O. & Dahn,J. R. Mechanically alloyed Sn–Fe(–C) powders as anode materials for Li ion batteries. III. Sn2Fe:SnFe3C active/inactive composites. J. Electrochem. Soc. 146, 423–427 (1999).
[43] Idota, Y., Kabuto, T., Matsufuji, A., Maekawa, Y. & Miyasaki, T. Tin-based amorphous oxides: a high-capacity lithium-ion storage material. Science 276, 1395–1397 (1997).
[44] V.A. Sethuraman, M.J. Chon, M. Shimshak, V. Srinivasan, and P.R. Guduru, In situ measurements of stress evolution in silicon thin films during electrochemical lithiation and delithiation, Journal of Power Sources, 195: 5062-5066. (2010)
[45] V.A. Sethuraman, M.J. Chon, M. Shimshak, N. Van Winkle, and P.R. Guduru, In situ measurements of the biaxial modulus of Si anode for Li-ion batteries, Electrochemistry Communications, 12: 1614-1617. (2010)
[46] Chen, J., et al., Mechanical analysis and in situ structural and morphological evaluation of Ni–Sn alloy anodes for Li ion batteries. Journal of Physics D: Applied Physics, 41(2): p. 025302. (2008)
[47] Y. Qi and S.J. Harris, In situ observation of strains during lithiation of a graphite electrode, Journal of The Electrochemical Society, 157(6): A741-A747. (2010)
[48] Okman, O., et al. In situ Observation of Cracking and Self-Healing in Li-Ion Battery Electrodes, Society of Engineering Science Annual Technical Meeting, Providence RI, July 28–31. (2013)
[49] Taeseup Song, Jianliang Xia, Jin-Hyon Lee, Dong Hyun Lee, Moon-Seok Kwon, Jae-Man Choi, Jian Wu, Seok Kwang Doo, Hyuk Chang, Won Il Park, Dong Sik Zang, Hansu Kim, Yonggang Huang, Keh-Chih Hwang, John A. Rogers, and Ungyu Paik NanoLetters 10 (5), 1710-1716 (2010)
[50] Jun Chen, Yong Liu, Andrew I. Minett, Carol Lynam, Jiazhao Wang,Gordon G. Wallace Chemistry of Materials 19 (15), 3595-3597 (2007)
[51] Li-Feng Cui, Liangbing Hu, Jang Wook Choi, and Yi Cui ACS Nano 4 (7), 3671-3678 (2010)

[52] Li Qiang Zhang, Xiao Hua Liu, Yang Liu, Shan Huang, Ting Zhu, Liangjin Gui, Scott X. Mao, Zhi Zhen Ye, Chong Min Wang, John P. Sullivan, and Jian Yu Huang ACS Nano 5 (6), 4800-4809 (2011)
[53] Jeannine R. Szczech and Song Jin Nanostructured silicon for high capacity lithium battery anodes Energy Environ. Sci., 2011, 4, 56-72
[54] M. Uehara, J. Suzuki, K. Tamura, K. Sekine and T. Takamura, J. Power Sources, 2005,146, 441–444
[55] T. Moon, C. Kim and B. Park, J. Power Sources, 2006, 155, 391–394
[56] B. K. Lee, G. B. Cho, K. K. Cho and K. W. Kim, Diffus. Defect Data, Pt. B, 2007, 124–126, 1011–1014
[57] T. Zhang, H. P. Zhang, L. C. Yang, B. Wang, Y. P. Wu and T. Takamura, Electrochim. Acta, 2008, 53, 5660–5664
[58] L. B. Chen, J. Y. Xie, H. C. Yu and T. H. Wang, J. Appl. Electrochem., 2009, 39, 1157–1162
[59] H. X. Deng, C. Y. Chung, Y. T. Xie, P. K. Chu, K. W. Wong, Y. Zhang and Z. K. Tang,Surf. Coat. Technol., 2007, 201, 6785–6788
[60] Teki, Ranganath, et al. "Nanostructured silicon anodes for lithium ion rechargeable batteries." Small 5.20 (2009): 2236-2242.
[61] Maranchi, J. P., et al. "Interfacial properties of the a-Si∕Cu: active–inactive thin-film anode system for lithium-ion batteries." Journal of the Electrochemical Society 153.6 (2006): A1246-A1253.
[62] M. Ignat, Chemical Vapor Deposition, ASM International, Surface Engineering Series, Vol. 2, J. Park, Editor, pp. 45-80, ASM International, Metals Park, OH
[63] J.L. Goldman, B.R. Long, A.A. Gewirth, and R.G. Nuzzo, Advanced Functional Materials, Volume 21, Issue 13, pages 2412–2422, (2011)
[64] Juchuan Li, et al. Crack Pattern Formation in Thin Film Lithium-Ion Battery Electrodes Journal of The Electrochemical Society, volume 158, issue 6, A689-A694 (2011)
[65]Bard, Allen J.; Larry R. Faulkner (2000-12-18). Electrochemical Methods: Fundamentals and Applications
[66] M Contestabile, S Panero, B Scrosati, A laboratory-scale lithium-ion battery recycling process, Journal of Power Sources, Volume 92, Issues 1–2, Pages 65-69, (2001)
[67] MA Sutton, WJ Wolters, WH Peters, WF Ranson, SR McNeill, Determination of displacements using an improved digital correlation method, Image and Vision Computing, Volume 1, Issue 3,Pages 133-139,(1983)
[68] SEM workshop University of South Carolina (2009)
[69] Tang Z, Liang J, Guo C, Wang Y; Photogrammetry-based two-dimensional digital image correlation with nonperpendicular camera alignment. Opt. Eng.51 (2) (2012)
[70] K.L. Mittal Electro Component Science and Technology Volume 3, Issue 1, Pages 21-42, (1976)
[71] J. Yuan and V. Gupta, J. Appl. Phys. 74. 2388 (1993)
[72] V. Gupta, and J. Yuan, J. Appl. Phys. 74. 2397 (1993)
[73] J. Yuan, V. Gupta, and A. Pronin J. Appl. Phys. 74. 2305 (1993)
[74] J. Wang, R. L. Weaver and N. Sottos. J. Appl. Phys. 93. 9529 (2003)
[75] Son, B., et al., Effect of cathode/anode area ratio on electrochemical performance of lithium-ion batteries. Journal of Power Sources, 243: p. 641-647. (2013)

[76] A. N. Buckley, R Woods, Aust. J. Chem. 1984, 37, 2403.

CURRICULUM VITA

Jubin Chen

Department of Mechanical Engineering
University of Louisville
Louisville, KY 40292
E-mail: jubinchen@yahoo.com

EDUCATIONAL BACKGROUND:

- **University of Louisville (Louisville, KY)**
  Ph.D in Mechanical Engineering, August 2015

- **Dalian University of Technology (Dalian, China)** December 2006
  Master in Engineering Mechanics

- **Dalian University of Technology (Dalian, China)** June 2003
  Bachelor in Engineering Mechanics

RESEARCH JOURNAL PUBLICATIONS:

- **Jubin Chen**, Arjun K. Thapa, Thomas A. Berfield *In-Situ* Characterization of Strain in Lithium Battery Working Electrodes Journal of Power Sources Vol. 271, 2014, pp 406-413
- Qianjin Yue, Xiaohui Ren, **Jubin Chen**. The test and mechanism investigate for ductile-to-brittle transition on sea ice, Journal of Basic Science and Engineering Vol.13 No.1 2005 pp35-42

CONFERENCE PRESENTATIONS:

- **Jubin Chen**, Thomas A. Berfield *In-Situ* Characterization of Strain in Lithium Ion Battery Anodes, SEM Annual conference, Lombard, IL June3-6, 2013

AWARDS:

- Doctoral dissertation completion award (2015)
- Grosscurth fellowship from J. B. Speed School at University of Louisville, 2006-2008.

PROFESSIONAL SOCIETY:

- Member of Society of Experimental Mechanics (SEM), 2013-2014.